Elementary Particle Physics

A Supplementary Guide for PHYS-472 Lectures by Asst. Prof. Bora Akgün

Cengizhan Koyutürk

Summer 2024

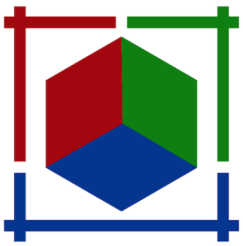

Contents

Introduction

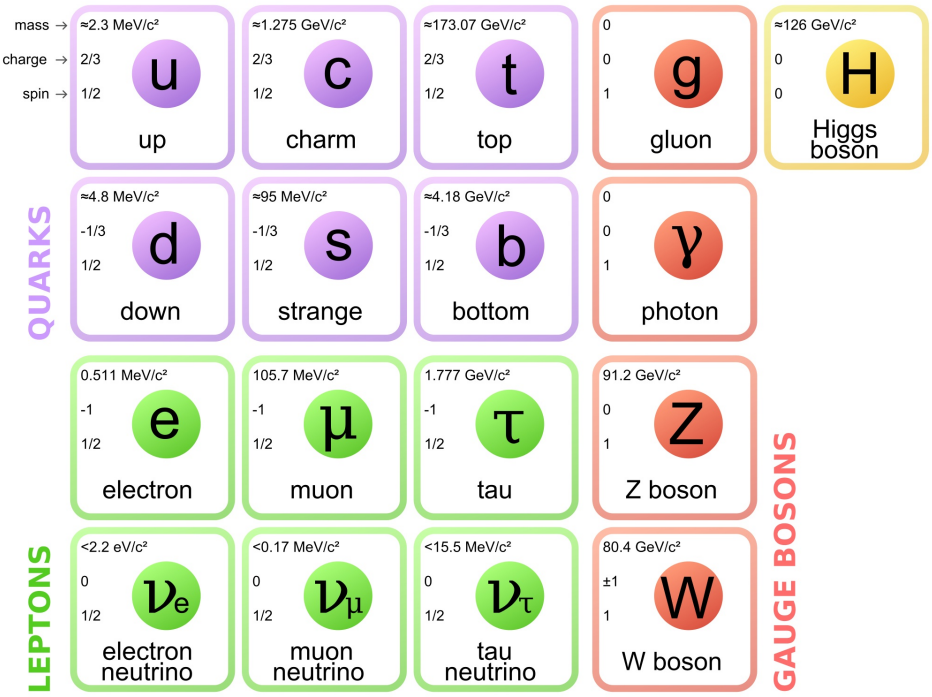

Figure 1.1: The Standard Model of Particle Physics.

Particle physics is a branch of science dedicated to understanding the most fundamental constituents of matter and the forces that govern their interactions. This field delves into the smallest scales of the universe, exploring particles that form the building blocks of everything around us. By investigating these elementary particles, scientists aim to uncover the underlying principles that constitute the fabric of the cosmos.

This book is based on the notes taken in the PHYS472 Elementary Particle Physics class at Boğaziçi University, taught by Asst. Prof. Bora Akgün. The course provides an introductory overview of the Standard Model and covers topics such as:

- Leptons, quarks, and hadrons
- Experimental methods

- Space-time symmetries
- Quantum chromodynamics (QCD), jets, gluons
- Weak interactions and electroweak unification
- Charge conjugation and parity (CP) violation
- Higgs Boson
- Discrete Symmetries

In addition to class notes, this book includes supplementary information from online sources and reference books provided in the syllabus, namely *"Particle Physics"* by B.R. Martin and G. Shaw, and *"Introduction to High Energy Physics"* by Donald H. Perkins. These sources offer further insights and detailed explanations, enriching the material covered in lectures.

Leptons and Quarks

In particle physics, two main categories of particles are studied: leptons and quarks. Leptons include familiar particles such as electrons, which orbit atomic nuclei, and neutrinos, which are incredibly elusive and challenging to detect. These particles are fundamental, meaning they are not composed of smaller components. Quarks, in contrast, combine in specific ways to form protons and neutrons, which are the core components of atomic nuclei. Unlike leptons, quarks never exist independently; they are always found in groups, held together by a strong nuclear force. Leptons and quarks form the basis of the Standard Model of particle physics, a well-established theory that describes their interactions.

Aim of the Book

This book aims to provide a comprehensive introduction to the field of particle physics. It is intended for students who are new to the subject as well as those who have an interest in the topic.

Fundamental Forces and Particle Interactions

Our discussion begins with the four fundamental forces that govern the behavior of particles: gravity, electromagnetism, the strong nuclear force, and the weak nuclear force. These forces dictate how particles interact, bind together, and decay into other particles, playing a crucial role in shaping the universe as we know it.

Gravity

Gravity is responsible for the attraction between masses. It is the weakest of the four forces but operates over infinite distances, governing the structure of the universe on a large scale. Described by Einstein's theory of general relativity, gravity revolutionized our understanding of how mass and energy influence the curvature of spacetime.

Electromagnetism

Electromagnetism acts between electrically charged particles and is responsible for electric and magnetic fields. It governs phenomena such as light, the behavior of atoms and molecules, and the binding of electrons to atomic nuclei. Electromagnetic interactions are described by quantum electrodynamics (QED), a highly successful theory that combines quantum mechanics and special relativity for the first time.

Strong Nuclear Force

The strong nuclear force binds quarks together to form protons, neutrons, and other hadrons. It is the strongest of the four forces, acting only over very short distances comparable to the size of an atomic nucleus. Quantum chromodynamics (QCD) describes the strong nuclear force, explaining how the exchange of particles called

gluons holds quarks together.

Weak Nuclear Force

The weak nuclear force is responsible for processes such as beta decay in radioactive atoms. It affects all fermions (particles with half-integer spin) and is crucial for the synthesis of elements in stars and the functioning of the sun. Described by the electroweak theory, it unifies with electromagnetism under a single theoretical framework.

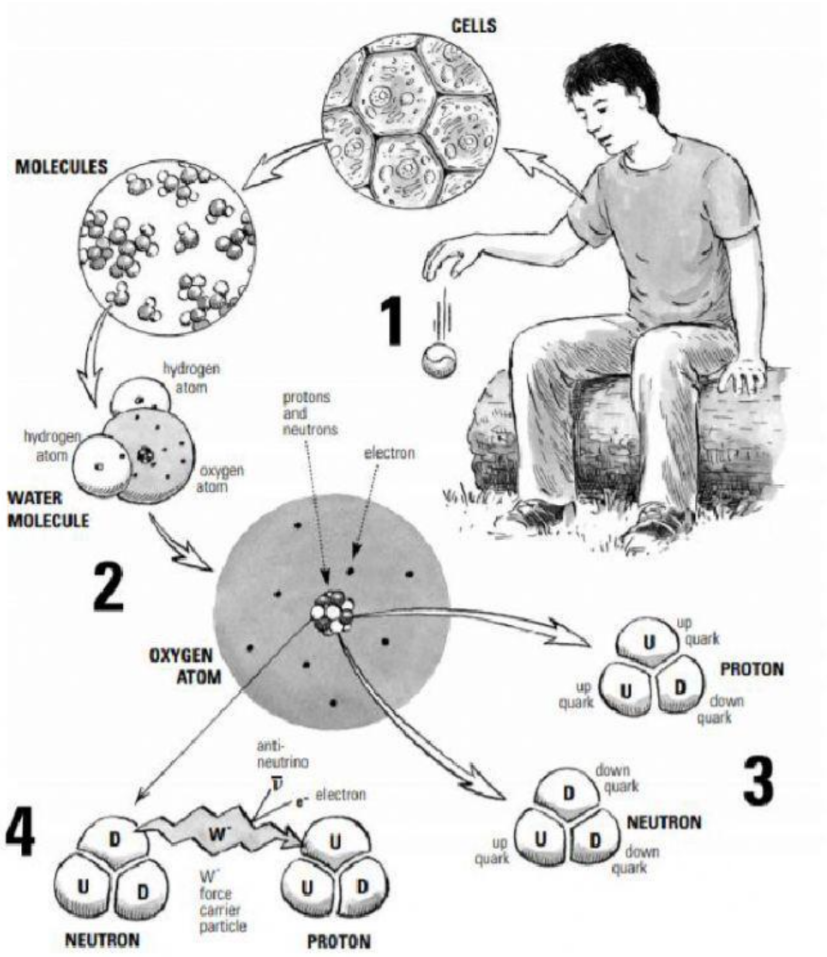

Figure 2.1: Diagram illustrating the four fundamental forces of nature.

Throughout this book, we will examine key concepts such as particle decay, conservation laws, and the processes occurring at the subatomic level. By exploring both theoretical frameworks and experimental evidence, we aim to provide a clear and comprehensive introduction to particle physics.

Leptons

Table 3.1: Leptons and Their Properties

Name	Symbol	Antiparticle	Charge (e)	Mass (MeV/c^2)
Electron	e^-	e^+	-1	$0.510998950 \pm 0.00000000015$
Electron Neutrino	ν_e	$\bar{\nu}_e$	0	$< 2.2 \times 10^{-6}$
Muon	μ^-	μ^+	-1	$105.6583755 \pm 0.0000023$
Muon Neutrino	ν_μ	$\bar{\nu}_\mu$	0	< 0.170
Tau	τ^-	τ^+	-1	1776.86 ± 0.12
Tau Neutrino	ν_τ	$\bar{\nu}_\tau$	0	< 15.5

Leptons are spin-$\frac{1}{2}$ particles. As shown above, they can be grouped into two different categories.

- **Neutrino**: Represented by ν in the upper indices, neutrinos are electrically neutral and do not interact via strong or electromagnetic forces[1]. Consequently, detecting and analyzing them is particularly challenging.
- **Electron, Muon, and Tau**: These particles each carry a -1 unit charge and interact via electromagnetic and weak forces. Among them, e^- is the least massive, while τ^- is the most massive. As their mass increases, their lifetime decreases. Consequently, electrons are more commonly observed than tau particles[2]. Each of these charged leptons has a corresponding antiparticle—positron (e^+), antimuon (μ^+), and antitau (τ^+)—which carry a +1 unit charge and behave similarly but with opposite charge and lepton number.

Muons interact with matter less than electrons, allowing them to penetrate more deeply into materials[3].

3.1 Lepton Number

Lepton number is a conserved quantum number[4] defined for leptons. It is assigned to each lepton family and remains constant in all interactions. The lepton number is +1 for leptons and -1 for antileptons. There are three

[1] Neutrinos only interact via the weak nuclear force, making them extremely difficult to detect and study.
[2] The lifetime of a particle is inversely related to its mass; more massive particles decay more quickly.
[3] Muons are often used in experiments to investigate the internal structure of materials due to their deep penetration.
[4] Conservation laws are fundamental principles in physics that state certain properties of an isolated system remain constant over time.

types of lepton numbers:

- **Electron Lepton Number (L_e)**: Conserved in interactions involving electrons and electron neutrinos.
- **Muon Lepton Number (L_μ)**: Conserved in interactions involving muons and muon neutrinos.
- **Tau Lepton Number (L_τ)**: Conserved in interactions involving taus and tau neutrinos.

Each type of lepton number is conserved separately in all types of interactions. For example, in the decay of a muon (μ^-), the muon lepton number before and after the decay remains the same, ensuring conservation. Similarly, the electron and tau lepton numbers are conserved in their respective interactions and decays.

Below, we provide examples of how more massive particles decay into their less massive counterparts, in accordance with conservation laws (charge, lepton number).

$$\mu^- \to e^- + \bar{\nu}_e + \nu_\mu \tag{3.1}$$

$$\mu^+ \to e^+ + \nu_e + \bar{\nu}_\mu \tag{3.2}$$

$$\tau^- \to \mu^- + \bar{\nu}_\mu + \nu_\tau \tag{3.3}$$

$$\tau^+ \to \mu^+ + \nu_\mu + \bar{\nu}_\tau \tag{3.4}$$

These reactions can be tested and verified to obey conservation laws. In equations 3.3 and 3.4, we could have used the expressions in equations 3.1 and 3.2 respectively, replacing the muon terms. However, this would introduce more neutrinos into our reactions and analysis. Given the difficulty of studying neutrinos, we adhere to these expressions[5].

3.1.1 Example: Conservation of Lepton Number

Let's demonstrate the conservation of the lepton number using the following reaction as an example:

$$\mu^- \to e^- + \bar{\nu}_e + \nu_\mu \tag{3.5}$$

1. Initial Lepton Number

We'll begin by analyzing the lepton number of the initial particle, which is the muon (μ^-).

[5]Neutrinos are notoriously difficult to detect because they interact very weakly with matter.

- **Muon Family (μ^-):** The muon belongs to the muon family, so its lepton number is:

$$L_\mu = +1 \tag{3.6}$$

- **Electron Family (μ^-):** The muon does not belong to the electron family, so its lepton number in the electron family is:

$$L_e = 0 \tag{3.7}$$

- **Tau Family (μ^-):** The muon does not belong to the tau family, so its lepton number in the tau family is:

$$L_\tau = 0 \tag{3.8}$$

- **Total Initial Lepton Number:**

$$L_{\text{initial, }\mu} = +1 \tag{3.9}$$

$$L_{\text{initial, }e} = 0 \tag{3.10}$$

$$L_{\text{initial, }\tau} = 0 \tag{3.11}$$

2. Final Lepton Number

Now let's analyze the lepton number for each particle on the right side of the reaction.

- **Electron (e^-):** The electron belongs to the electron family, so its lepton number is:

$$L_e = +1 \tag{3.12}$$

- **Electron Antineutrino ($\bar{\nu}_e$):** The electron antineutrino is the antiparticle of the electron neutrino, so it has a lepton number of:

$$L_e = -1 \tag{3.13}$$

- **Muon Neutrino (ν_μ):** The muon neutrino belongs to the muon family, so its lepton number is:

$$L_\mu = +1 \tag{3.14}$$

- **Tau Family:** None of the final particles belong to the tau family, so their lepton number in this family is:

$$L_\tau = 0 \tag{3.15}$$

- **Lepton Number of Each Family:**

$$L_{\text{final, }e} = +1 + (-1) = 0 \tag{3.16}$$

$$L_{\text{final},\,\mu} = +1 \tag{3.17}$$

$$L_{\text{final},\,\tau} = 0 \tag{3.18}$$

3. Conservation Check

Let's check if the lepton numbers are conserved for each family:

Lepton Family	Initial Lepton Number	Final Lepton Number	Conserved?
Muon Family (μ)	$+1$	$+1$	Yes
Electron Family (e)	0	0	Yes
Tau Family (τ)	0	0	Yes

Table 3.2: Lepton Number Conservation Check

Since the initial and final lepton numbers are equal for each family, the lepton number is **conserved** in this reaction.

3.2 Branching Ratios

Branching ratios indicate the likelihood of a particle decaying into a particular final state. For instance, the branching ratio for the decay of a tau lepton (τ^-) into a muon (μ^-) and two neutrinos ($\bar{\nu}_\mu$ and ν_τ) can be expressed as:

$$\mathcal{B}(\tau^- \to \mu^- + \bar{\nu}_\mu + \nu_\tau) = (17.39 \pm 0.04)\% \tag{3.19}$$

This means that approximately 17.39% of tau leptons will decay into this specific final state, with small uncertainty. Branching ratios are crucial for predicting the outcomes of particle interactions and for comparing theoretical models with experimental data.

3.3 Lepton Universality

Lepton universality states that the interaction mechanisms for leptons are independent of their generation. This means that the fundamental interactions are the same for electrons, muons, and tau particles, apart from differences due to their masses. An example illustrating lepton universality is the decay of a W boson (W^-):

$$W^- \to e^- + \bar{\nu}_e \quad (10.71 \pm 0.16)\% \tag{3.20}$$

$$W^- \to \mu^- + \bar{\nu}_\mu \quad (10.63 \pm 0.15)\% \tag{3.21}$$

$$W^- \to \tau^- + \bar{\nu}_\tau \quad (11.38 \pm 0.21)\% \tag{3.22}$$

These decays occur with approximately the same probability, demonstrating that the weak interaction does not distinguish between the different generations of leptons. This principle is a cornerstone of the electroweak theory and is supported by experimental evidence.

3.4 Visualization in CMS

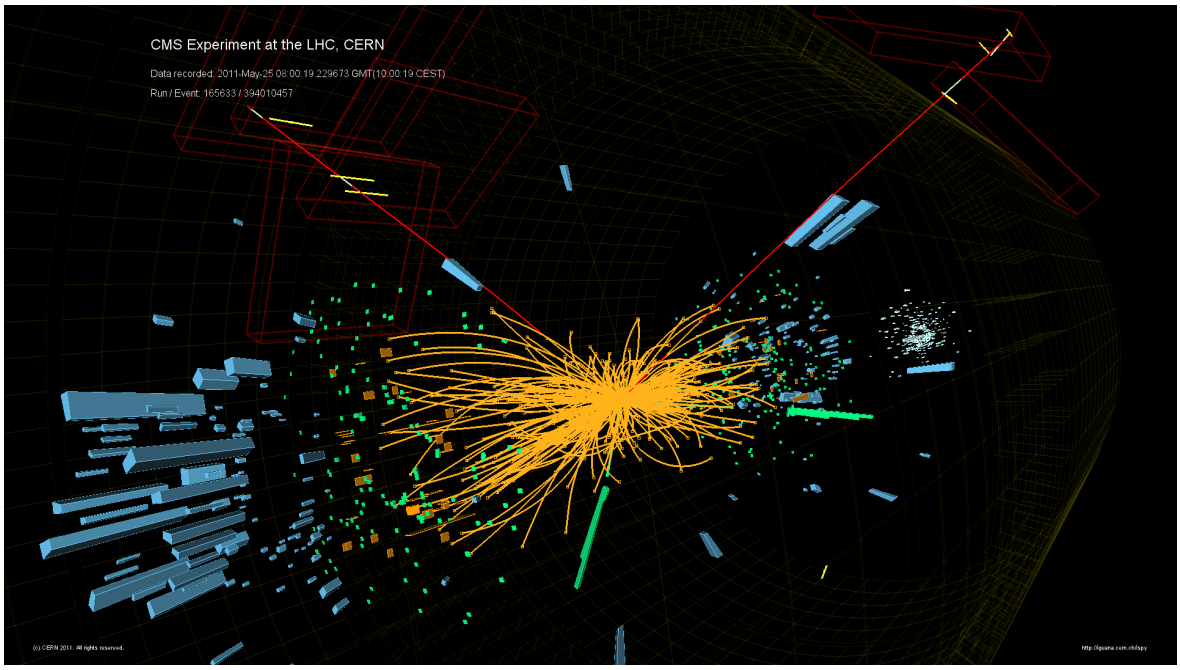

Figure 3.1: Visualization from the CMS detector, showing various particle tracks and energy deposits.

The CMS detector at the LHC provides visualizations of particle interactions. In these visualizations, as shown in Figure 3.1, **red lines** typically represent the tracks of muons, which are minimally interacting particles capable of penetrating all detector layers. **Green bars** indicate the energy deposits in the electromagnetic calorimeter (ECAL), primarily from electrons and photons.

Leptonic Weak Interactions

4.1 Leptonic Weak Interactions

Leptonic weak interactions involve the exchange of W and Z bosons[1], mediating processes such as beta decay and neutrino scattering[2]. Feynman diagrams effectively illustrate these decay processes. Let's analyze Figure 4.1 part by part.

4.2 Feynman Diagrams of Neutrino Interactions

(a) Interaction via Z^0.

(b) Interaction via W^-.

Figure 4.1: Feynman diagrams showing neutrino interactions.

First, consider an incident electron interacting with a muon neutrino via a Z^0 boson, as shown in Figure 4.1a. The electron and neutrino retain their initial charges because the Z^0 boson does not carry any charge. This interaction, also known as an elastic collision[3], conserves both charge and lepton numbers.

Next, examine Figure 4.1b, which depicts an inverse muon decay[4]. An electron emits a W^- boson and transi-

[1] W and Z bosons are the force carriers of the weak interaction, analogous to how photons are the force carriers of the electromagnetic interaction.

[2] Beta decay is a type of radioactive decay in which a neutron transforms into a proton, or vice versa, emitting an electron or positron and a neutrino or antineutrino. Neutrino scattering involves neutrinos interacting with other particles, providing insight into their properties.

[3] An elastic collision is a collision in which kinetic energy is conserved.

[4] Inverse muon decay is a process where a muon neutrino interacts with an electron, leading to the production of a muon and an electron

tions into an electron neutrino. The W^- boson is then absorbed by a muon neutrino, which becomes a muon. In both diagrams, time progresses from left to right, following the convention for Feynman diagrams.

4.3 Zero-Range Interaction Concept

Now, by studying one of the examples given in the previous section, we can introduce the concept of zero-range interaction.

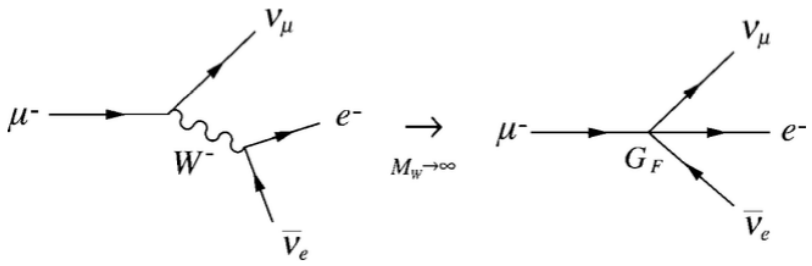

Figure 4.2: Origin of the low-energy zero-range interaction in muon decay.

In Figure 4.2, we analyze a Feynman diagram for muon decay. An incident muon emits a W^- boson and transitions into a muon neutrino. Subsequently, an anti-electron neutrino absorbs the W^- boson, transforming into an electron.

At the energy scales relevant to this interaction, the de Broglie wavelength of the particles is relatively long compared to the range of the W^- boson[5]. Consequently, we can approximate this force as if it occurred at a single point. The strength of this interaction is characterized by the Fermi constant G_F[6], which quantifies the coupling strength of the weak force at low energies.

4.4 Flavor Change and Weak Interactions

The weak force is unique among the fundamental forces due to its ability to change the flavor of quarks and leptons. This property is crucial for processes such as beta decay, where a neutron decays into a proton, electron, and an anti-electron neutrino[7]. The Fermi constant plays a vital role in calculating the rates of these weak interaction processes.

In summary, leptonic weak interactions are essential for understanding fundamental particle decays and interactions. Feynman diagrams provide a visual representation of these processes, highlighting the exchange of W and Z bosons and the conservation of quantum numbers.

neutrino.

[5]The de Broglie wavelength is a fundamental concept in quantum mechanics, representing the wave-like behavior of particles. For particles with low momentum, the wavelength is long.

[6]The Fermi constant G_F is a measure of the strength of weak interactions. It is fundamental in calculating the probabilities of processes mediated by the weak force.

[7]Flavor change refers to the transformation of one type of quark or lepton into another. In beta decay, a down quark in a neutron changes to an up quark, converting the neutron into a proton.

Quarks and Their Properties

Table 5.1: Quarks and Their Properties.

Name	Symbol	Antiparticle	Charge (e)	Mass (MeV/c^2)
Up	u	$\bar{u}$	$+\frac{2}{3}$	$2.16^{+0.49}_{-0.26}$
Down	d	$\bar{d}$	$-\frac{1}{3}$	$4.67^{+0.48}_{-0.17}$
Charm	c	$\bar{c}$	$+\frac{2}{3}$	$1,275 \pm 25$
Strange	s	$\bar{s}$	$-\frac{1}{3}$	93^{+11}_{-5}
Top	t	$\bar{t}$	$+\frac{2}{3}$	$172,700 \pm 600$
Bottom	b	$\bar{b}$	$-\frac{1}{3}$	$4,180 \pm 30$

5.1 Quark Generations and Properties

The known quarks are given above. Each column is referred to as a **generation**, and each entry within a generation is called a *flavor*. The upper flavors have an electric charge of $\frac{2}{3}$, while the lower flavors have an electric charge of $\frac{-1}{3}$. All quarks possess the same spin[1] ($\frac{1}{2}$). The average mass of the quarks increases as we move from left to right across the generations. On the far right, the top quark (t) has the highest mass, whereas the up quark (u) on the far left has the lowest mass. Due to their substantial masses, top and bottom quarks are rarely observed, as they tend to decay into less massive states.

5.2 Generations of Quarks

5.2.1 First Generation

The up (u) and down (d) quarks make up the first generation. These quarks are the least massive and most stable, forming the building blocks of protons and neutrons. Up quarks have a charge of $\frac{2}{3}$, while down quarks carry a charge of $\frac{-1}{3}$. The proton (uud) and neutron (udd) are composed of these quarks.

[1] Spin is a fundamental property of particles, akin to angular momentum, which determines the particle's intrinsic rotation.

5.2.2 Second Generation

The charm (c) and strange (s) quarks are part of the second generation. Charm quarks have a charge of $\frac{2}{3}$ and are significantly more massive than up quarks. Strange quarks, with a charge of $\frac{-1}{3}$, are slightly more massive than down quarks. Mesons such as D mesons ($c\bar{u}$, $c\bar{d}$) and K mesons ($u\bar{s}$, $d\bar{s}$) contain these quarks.

5.2.3 Third Generation

The top (t) and bottom (b) quarks form the third generation. These quarks are the most massive, with the top quark being the most massive of all quarks, having a charge of $\frac{2}{3}$. Bottom quarks have a charge of $\frac{-1}{3}$. Due to their large masses, these quarks decay rapidly into less massive quarks. Particles such as B mesons ($b\bar{u}$, $b\bar{d}$) and the Υ meson ($b\bar{b}$) involve these quarks.

5.3 Quark Confinement

Quarks are never found in isolation due to a phenomenon called confinement[2]. They are always bound together by the strong force, mediated by gluons[3], to form composite particles known as hadrons. This binding is so strong that attempting to separate quarks results in the creation of new quark-antiquark pairs.

5.4 Color Charge

Quarks carry a property known as color charge, which is analogous to electric charge but comes in three types: red, green, and blue[4]. Gluons, the force carriers of the strong interaction, exchange color charge between quarks, ensuring that hadrons are always color-neutral. This is different from electric charge, which only comes in positive and negative forms.

5.5 Mass and Decay

The masses of quarks vary widely. The top quark, being the most massive, has a mass of $172.7 \pm 0.6\,\mathrm{GeV}/c^2$, while the up quark is the least massive, with a mass of $2.16^{+0.49}_{-0.26}\,\mathrm{MeV}/c^2$. Quarks decay into other quarks through weak interactions, changing their flavor in the process. For example, a top quark can decay into a bottom quark by emitting a W^+ boson, which then decays into a positron and a neutrino.

Understanding the properties and interactions of quarks is crucial for the study of particle physics. The behavior of quarks under the strong force explains the stability and structure of protons and neutrons, and their interactions give rise to the vast array of particles observed in high-energy experiments.

[2] Quark confinement refers to the fact that quarks cannot be separated from each other; they are always found in groups forming hadrons.
[3] Gluons are the force carriers of the strong interaction, responsible for binding quarks together.
[4] Color charge is a property of quarks related to the strong interaction, similar to how electric charge is related to the electromagnetic interaction.

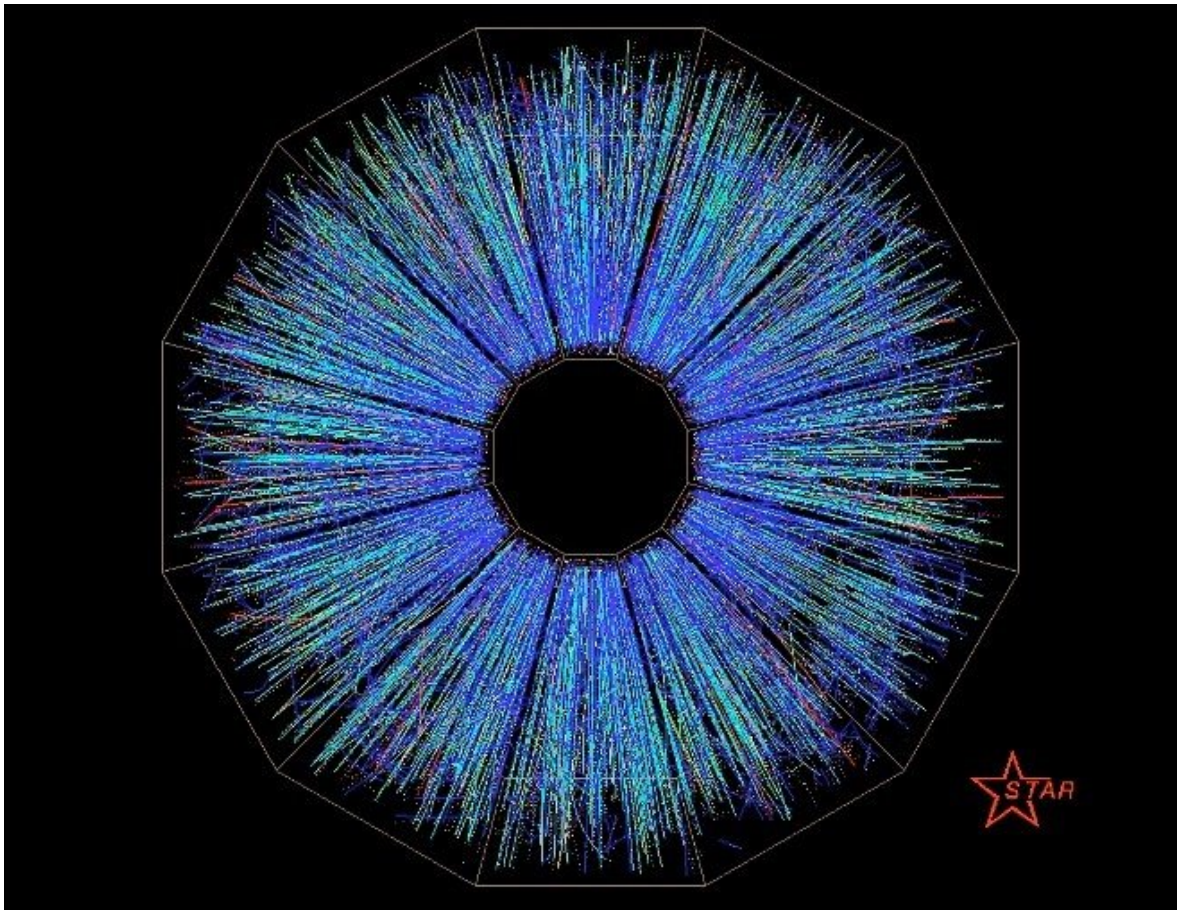

Figure 5.1: An image of the debris left over after the creation of quark-gluon plasma in the collision of two nuclei at Brookhaven National Laboratory.

General Properties of Hadrons

Quarks and leptons are fundamental particles in the Standard Model. While leptons interact via electromagnetic and weak forces, quarks interact primarily through the strong force, mediated by gluons. Quarks have fractional electric charges and cannot exist in isolation due to confinement, forming bound states known as hadrons. There are three main types of hadrons:

6.1 Types of Hadrons

6.1.1 Baryons

Baryons are particles composed of three quarks. These quarks combine to form a particle with a half-integer spin. Examples of baryons include protons, composed of two up quarks and one down quark (uud), and neutrons, composed of one up quark and two down quarks (udd). Baryons are some of the most stable particles due to their quark structure, and they make up the nuclei of atoms.

6.1.2 Antibaryons

Antibaryons are the antiparticles of baryons, consisting of three antiquarks. Each antiquark has the opposite quantum numbers of its corresponding quark. For example, the antiproton ($\bar{p}$) consists of two anti-up quarks and one anti-down quark ($\bar{u}\bar{u}\bar{d}$). Like baryons, antibaryons have half-integer spin, making them fermions. When baryons and antibaryons meet, they annihilate each other, producing energy.

6.1.3 Mesons

Mesons are particles consisting of one quark and one antiquark ($q\bar{q}$), resulting in integer spins, classifying them as bosons. Mesons play a crucial role in mediating the strong force between baryons in the atomic nucleus. An example of a meson is the pion (π^+), composed of an up quark and an anti-down quark ($u\bar{d}$). Mesons are generally less stable than baryons and decay into particles with lesser masses.

These hadrons possess different quantum numbers based on their quark content. Table 6.1 shows the quantum numbers for several baryons.

Particle	Quark Content	Mass (MeV/c^2)	Q (Charge)	S (Strangeness)	C (Charm)	B (Bottomness)
p (Proton)	uud	938.272 ± 0.0005	$+1$	0	0	0
n (Neutron)	udd	939.565 ± 0.0005	0	0	0	0
Λ	uds	1115.683 ± 0.006	0	-1	0	0
Λ_c^+	udc	2286.46 ± 0.14	$+1$	0	$+1$	0
Λ_b^0	udb	5619.60 ± 0.17	0	0	0	-1

Table 6.1: Properties of Various Baryons.

6.2 Quantum Numbers

Here, Q denotes the electric charge, S represents strangeness, C indicates charm, and $\tilde{B}$ corresponds to the bottom quantum number. Another important quantum number, denoted by T, is not included in this table. These quantum numbers can be determined using the following formulas:

$$S \equiv -N_s \equiv -[N(s) - N(\bar{s})], \tag{6.1}$$

$$C \equiv N_c \equiv N(c) - N(\bar{c}), \tag{6.2}$$

$$\tilde{B} \equiv -N_b \equiv -[N(b) - N(\bar{b})], \tag{6.3}$$

$$T \equiv N_t \equiv N(t) - N(\tilde{t}), \tag{6.4}$$

To illustrate, consider the proton (*uud*). It contains zero strange (s and $\bar{s}$), charm (c and $\bar{c}$), and bottom (b and $\bar{b}$) quarks. Therefore, the S, C, and $\tilde{B}$ quantum numbers are zero. Summing the electric charges of two u quarks and one d quark gives a total electric charge of +1, corresponding to a Q value of 1. The baryon number (B) is given by:

$$B \equiv \frac{1}{3}[N(q) - N(\bar{q})], \tag{6.5}$$

6.3 Beta Decay

Now, let us consider the β-decay process depicted in Figure 6.1.

Initially, the neutron consists of one u quark and two d quarks. The electric charge (Q) is 0, and the baryon number (B) is 1. After the decay, a proton (uud), an electron, and an antineutrino are produced. The electric

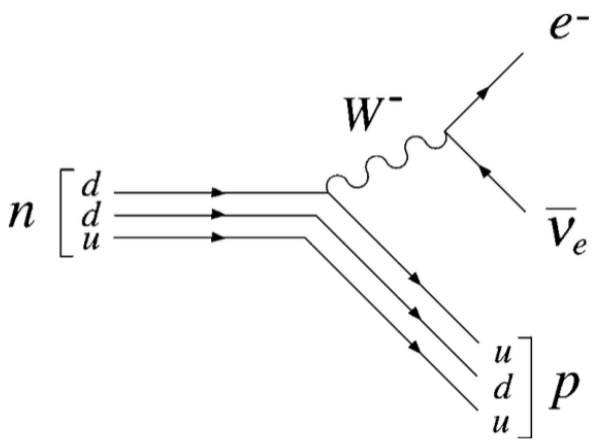

Figure 6.1: Quark diagram for the decay $n \to p + e^- + \bar{\nu}_e$.

charge and baryon number are conserved in this process, although the individual quark numbers are not because one d quark transforms into a u quark. In weak interactions, quark numbers may not be conserved, but electric charge and baryon numbers are always conserved.

The weak interaction responsible for beta decay is mediated by the W^- boson, which allows for the transformation of one type of quark into another. This process highlights the fundamental asymmetry in the weak force, differentiating it from the strong and electromagnetic forces, which do not change the type (flavor) of quarks involved.

Pions and Nucleons

7.1 Pions

Pions are the least massive known mesons. They can be electrically charged, $\pi^{\pm}(139.57039 \pm 0.00018$ MeV/c^2), or neutral, $\pi^0(134.9768 \pm 0.0005$ MeV/c^2). Pions play a crucial role in mediating the strong nuclear force within atomic nuclei. They can be produced through baryon-baryon collisions or in high-energy particle collisions.

7.2 Pion Production

Pions are produced in various types of particle collisions, such as baryon-baryon and proton-proton collisions. These processes are crucial in high-energy physics, as they provide insights into the strong interaction.

$$p + p \to p + n + \pi^+ \quad \textbf{or} \quad p + p \to p + p + \pi^0 \tag{7.1}$$

These reactions are permitted due to the conservation of several quantum numbers:

- **Baryon Number**: Conserved as the total baryon number before and after the collision remains the same.
- **Charge**: The total charge is conserved; for example, in the reaction $p + p \to p + n + \pi^+$, the charge remains $+2$ both before and after the collision.
- **Isospin**: The strong interaction preserves isospin, ensuring that the total isospin quantum number is conserved in the process.
- **Parity**: Parity is conserved in strong interactions, with the final state maintaining the required symmetry properties.

These conservation laws explain why pion production is commonly observed in particle accelerators and other high-energy experiments. The concepts of **isospin** and **parity** will be discussed in later sections.

7.3 Pion Decay

7.3.1 Charged Pions

Charged pions are unstable and decay primarily into muons and muon neutrinos. These decays are mediated by the weak force.

$$\pi^+ \to \mu^+ + \nu_\mu \tag{7.2}$$

$$\pi^- \to \mu^- + \bar{\nu}_\mu \tag{7.3}$$

The charged pions have a relatively short lifetime of about $2.6033 \times 10^{-8} \pm 0.0005 \times 10^{-8}$ seconds before decaying into muons.

7.3.2 Neutral Pions

Neutral pions decay via electromagnetic interaction, primarily into two photons. This process occurs very rapidly, with a lifetime of about $8.43 \times 10^{-17} \pm 0.13 \times 10^{-17}$.

$$\pi^0 \to \gamma + \gamma \tag{7.4}$$

The neutral nature of these pions makes them harder to detect because they do not leave any direct tracks in detectors. However, they can be identified by observing their decay photons.

7.4 Quark-Level Description of Pion Decay

Using Feynman diagrams[1], we can examine Equation 7.2 in terms of quarks:

$$(u\bar{d}) \to \mu^+ + \nu_\mu \tag{7.5}$$

In this process, a u quark annihilates with a $\bar{d}$ quark, resulting in an antimuon and a muon neutrino. This is illustrated in Figure 7.1 with the help of Feynman diagrams.

Once again, we observe that the quark numbers are not conserved, a characteristic feature of weak interactions[2]. The weak interaction allows for quark flavor change, which is essential in processes such as beta decay.

[1] Feynman diagrams are graphical representations used in particle physics to visualize and calculate interactions between particles.
[2] Weak interactions are one of the four fundamental forces of nature, responsible for processes like beta decay in radioactive atoms.

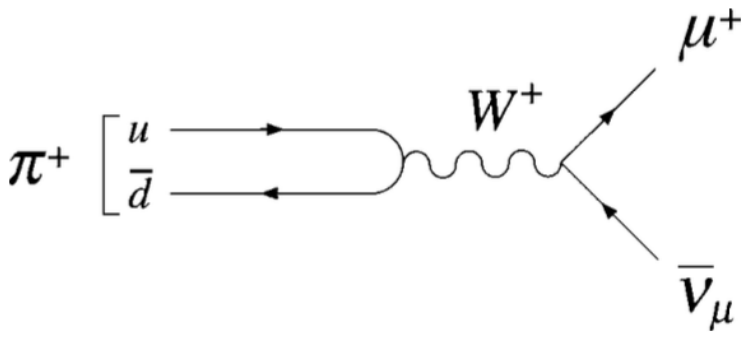

Figure 7.1: Quark diagram for the decay $\pi^+ \to \mu^+ + \nu_\mu$.

7.5 Nucleons

Nucleons, consisting of protons and neutrons, are the building blocks of atomic nuclei. Protons are composed of two up quarks and one down quark (uud), while neutrons consist of two down quarks and one up quark (udd). The interactions within nucleons, binding quarks together, are mediated by gluons, which are the carriers of the strong force.

7.5.1 Proton and Neutron Properties

Protons have a positive electric charge (+1), while neutrons are electrically neutral. The masses of protons and neutrons are nearly identical, with protons having a mass of $938.272 \pm 0.0005\,\text{MeV}/c^2$ and neutrons slightly more massive at $939.565 \pm 0.0005\,\text{MeV}/c^2$. The slight mass difference is critical for the stability of atomic nuclei and the processes of nuclear decay.

7.5.2 Nuclear Forces

The residual strong force, or nuclear force, binds protons and neutrons together within the nucleus. This force is effective over short distances and is responsible for the stability of nuclei. The strong force, mediated by gluons, binds quarks together within nucleons and also facilitates the interaction between nucleons, allowing them to stay bound within the atomic nucleus despite the repulsive electromagnetic force between protons.

Strange Particles, Charm, and Bottom

In 1947, a significant breakthrough occurred in particle physics with the discovery of strange particles. These particles were first observed by Rochester and Butler in cosmic ray experiments conducted at the University of Manchester. The discovery was notable because these particles were produced via strong interactions but exhibited unexpectedly long lifetimes, decaying via weak interactions. This behavior was unusual because particles produced through strong interactions were expected to decay rapidly. Due to their unexpected nature, these particles were termed ”strange particles.” The discovery of strange particles marked the beginning of a deeper understanding of the quark model and the development of quantum chromodynamics (QCD).

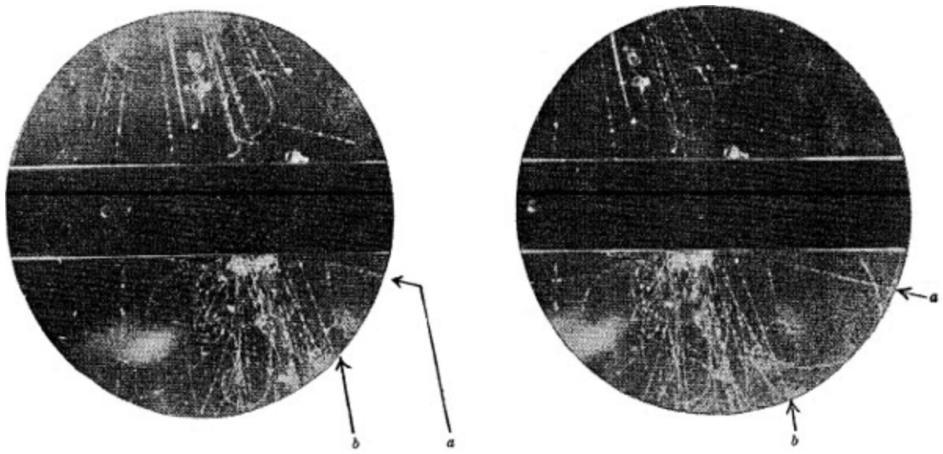

Figure 8.1: Stereoscopic photographs showing an unusual fork (a, b) in the gas. The direction of the magnetic field is such that a positive particle coming downwards is deviated in an anticlockwise direction.

Figure 8.1 shows the first observation of these particles. Stereoscopic photographs showing an unusual fork (a, b) in the gas. The direction of the magnetic field is such that a positive particle coming downwards is deviated in an anticlockwise direction. It depicts a positively charged particle with a mass of $493.677 \pm 0.016\,\mathrm{MeV}/c^2$ decaying into an antimuon and a muon neutrino. This process can be represented by the following equation and branching ratio[1]:

[1]The branching ratio B is the fraction of the total number of decays that follow a particular decay mode.

$$K^+ \to \mu^+ + \nu_\mu, \quad B = 63.56\% \pm 0.11\% \tag{8.1}$$

Another possible reaction is:

$$K^+ \to \pi^+ + \pi K^+ \to \pi^+ + \pi^0, \quad B = 20.67\% \pm 0.08\% \tag{8.2}$$

The particle on the left-hand side of the reaction is called a *kaon*, the least massive known strange meson. Its quark structure is $u\bar{s}$. Following this, we introduce the least massive known strange baryon, the Λ particle, composed of uds quarks. Strange quarks in Λ particles decay via weak interactions, so quark flavor conservation is not expected in the following decays:

$$\Lambda \to \pi^0 + n, \quad B = 35.8\% \pm 0.5\% \tag{8.3}$$

The Λ particle initially has a strangeness $S = -1$, as it contains a strange quark. However, during the decay process, the strange quark is transformed into a quark of a different flavor, resulting in a neutron (n) and a neutral pion (π^0), both of which have a strangeness $S = 0$. This illustrates that weak interactions do not conserve strangeness, allowing the strangeness quantum number to change during the decay.

8.1 Kaons and Associated Production

Kaons come in both charged and neutral forms, represented by their quark compositions:

$$K^+ = u\bar{s}, \quad K^- = \bar{u}s, \quad K^0 = d\bar{s}, \quad \bar{K^0} = \bar{d}s \tag{8.4}$$

Strange particles are produced via strong interactions, typically in *associated production*[2] processes where more than one strange particle is produced to obey conservation laws. For example:

$$\pi^- + p \to K^0 + \Lambda \tag{8.5}$$

In the reaction above, a neutral kaon and a lambda particle are produced. Initially, the total strangeness (S) and charge (Q) were both zero. On the right-hand side, the total charge remains zero. To determine the strangeness, we examine the quark compositions. The kaon (K^0) contains a $\bar{s}$ quark, contributing $S = +1$. The lambda particle (Λ) contains an s quark, contributing $S = -1$. Thus, the total strangeness remains zero, and the conservation law holds. This process is depicted in Figure 8.2.

[2] Associated production is a process in particle physics where strange particles are produced in pairs to conserve strangeness.

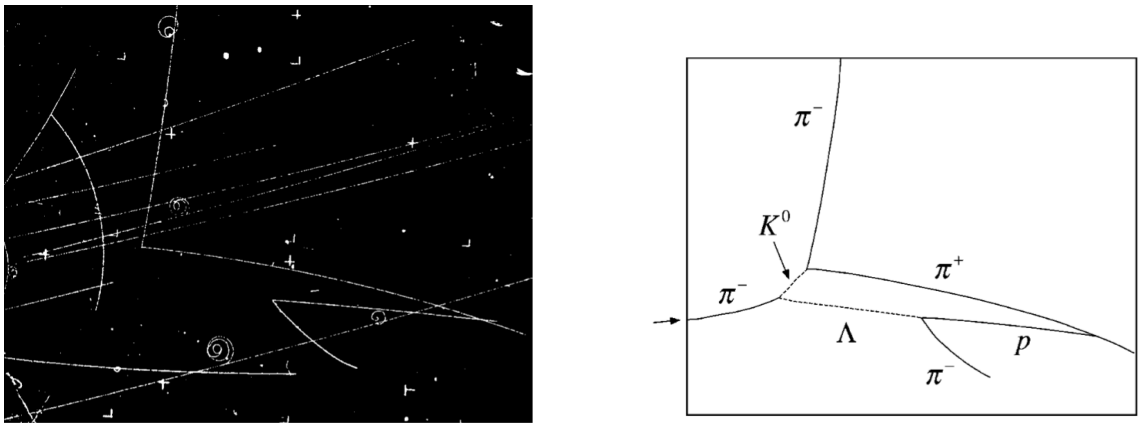

(a) (b)

Figure 8.2: Neutral Kaon and Lambda Production from Pion and Proton. (a) Image of the particle tracks in a bubble chamber. (b) Schematic diagram illustrating the production process.

8.2 Charm and Bottom Quarks

Until 1974, all discovered particles were bound states of u, d, and s quarks. This changed with the discovery of charmonium:

$$J/\Psi = c\bar{c} \tag{8.6}$$

The discovery, made independently by Brookhaven National Laboratory (BNL) and Stanford Linear Accelerator Laboratory (SLAC), refers to "charmonium" as analogous to "positronium," a bound state of a positron and an electron. Since the charm number of charmonium is zero, it is termed "hidden charm." There are also states with nonzero charm numbers, known as "naked charm."

The least massive charm mesons are:

$$D^+ = c\bar{d}, \quad D^- = \bar{c}d, \quad D^0 = c\bar{u}, \quad \bar{D}^0 = \bar{c}u \tag{8.7}$$

The masses of these particles are approximately D^+ and D^0 both around 1869.66 ± 0.05 MeV.

Additionally, D_s mesons involve both charm and strange quarks:

$$D_s^+ = c\bar{s}, \quad D_s^- = \bar{c}s \tag{8.8}$$

The mass of D_s^+ is about 1968.35 ± 0.07 MeV.

The quark composition of the least massive charmed baryon is:

$$\Lambda_c^+ = udc \tag{8.9}$$

The mass of Λ_c^+ is approximately 2286.46 ± 0.14 MeV. These particles have lifetimes on the order of 10^{-13} seconds, consistent with weak decays.

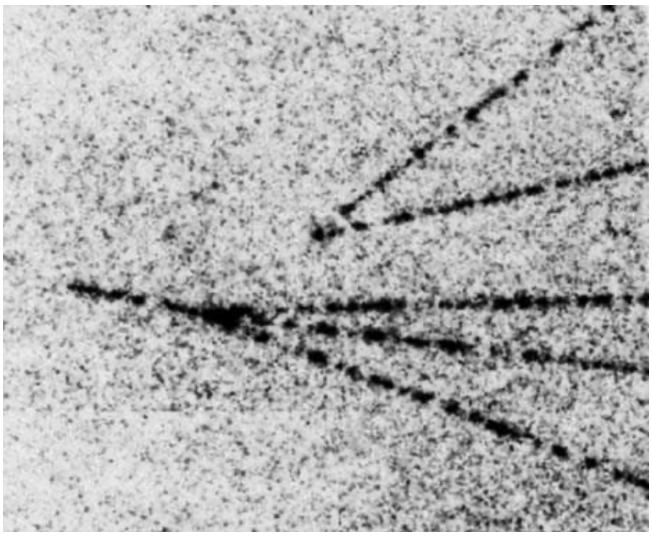

Figure 8.3: Production of Charmed Particles in a Bubble Chamber.

In a high-resolution bubble chamber at SLAC, an incident photon interacts with a proton, producing a charged charmed particle that decays after 2 mm into three charged particles, and a neutral charmed particle that decays after 3 mm into two charged particles.

We know there are six quarks in total. This became evident when the electromagnetic and weak forces were unified into the electroweak force, requiring an equal number of leptons and quarks. In 1977, the bottom quark (b) was discovered by Nobel laureate Leon Lederman at Fermilab. The first particle containing this quark was bottomonium:

$$\Upsilon = b\bar{b} \tag{8.10}$$

This particle is a meson in the state called "hidden bottom." The mass of Υ is about 9460.30 ± 0.26 MeV. The least massive bottom mesons are:

$$B^+ = u\bar{b}, \quad B^- = b\bar{u}, \quad B^0 = b\bar{d}, \quad \bar{B}^0 = d\bar{b} \tag{8.11}$$

These particles are in the state "naked bottom" with masses around B^+ and B^0 both about 5279.65 ± 0.12 MeV, with a lifetime of order 10^{-12} seconds.

An example of a bottom baryon is:

$$\Lambda_b^0 = udb \tag{8.12}$$

The mass of Λ_b^0 is approximately 5619.60 ± 0.17 MeV.

T mesons are hypothetical mesons composed of a top quark (t) and an antiquark from any other flavor (e.g., up,

down, strange, charm, or bottom). Because the top quark decays extremely quickly, T mesons are not expected to be found in nature. The quick decay of the top quark prevents the formation of stable T mesons, making them an interesting yet unattainable subject in high-energy particle physics.

Short-Lived Hadrons

Starting in the 1960s, high-energy collisions in laboratories revealed that hadrons decay via strong interactions rather than weak ones, with an average lifetime of approximately 10^{-23} seconds. Hadrons produced through these mechanisms are known as *resonances*.

9.1 Production and Detection of Resonances

Resonances are produced in high-energy collisions, as illustrated in Figure 9.1.

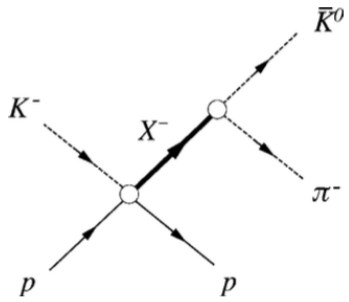

Figure 9.1: Production of a negatively charged resonance X^-.

Figure 9.1 shows the production of the X^- resonance from the reaction:

$$K^- + p \rightarrow X^- + p \tag{9.1}$$

Due to the extremely short lifetimes of resonances, direct detection is challenging. Instead, we measure the energy and momentum of the final particles from the decay reaction:

$$X^- \rightarrow \bar{K}^0 + \pi^- \tag{9.2}$$

From this, we infer the invariant mass[1] of the resonance X^- using energy-momentum conservation:

$$W^2 = (E_{\bar{K}^0} + E_{\pi^-})^2 - (\mathbf{p}_{\bar{K}^0} + \mathbf{p}_{\pi^-})^2 \tag{9.3}$$

Here, W is the invariant mass of the $K^0\pi^-$ system, $E_{\bar{K}^0}$ and E_{π^-} are the energies of the $\bar{K}^0$ and π^-, and $\mathbf{p}_{\bar{K}^0}$ and $\mathbf{p}_{\pi^-}$ are their respective momenta.

9.2 Invariant Mass Distribution

By analyzing the final states of particles, such as $\bar{K}^0$ and π^-, the invariant mass W of the system can be reconstructed. The invariant mass is calculated using the formula mentioned in (9.3).

When plotting the distribution of the invariant mass W of the $K^0\pi^-$ system, peaks appear at specific mass values corresponding to different resonances. These peaks are associated with the creation of short-lived hadrons, which subsequently decay into more stable particles. The width of the peak indicates the resonance's lifetime—the broader the peak, the shorter the lifetime of the resonance.

Figure 9.2 illustrates the invariant mass distribution for the X^- resonance, where a prominent peak is observed around 890 MeV. This peak signifies the resonance's presence, and the width of approximately 50 MeV reflects its decay properties.

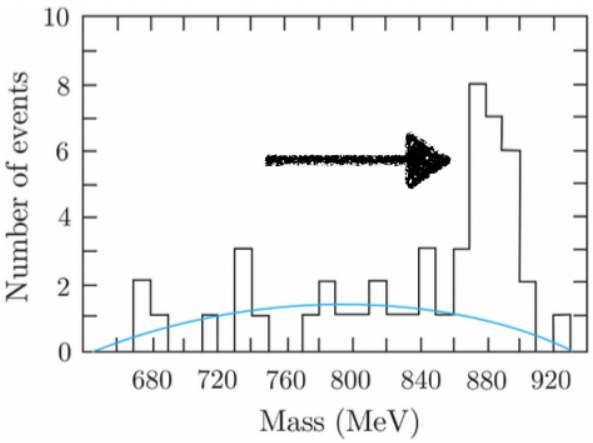

Figure 9.2: Invariant mass distribution of X^-.

9.3 Breit-Wigner Formula

The Breit-Wigner formula is used to analyze the width values of resonances. The formula is given by:

$$N(W) = \frac{K}{(W - W_r)^2 + \Gamma^2/4} \tag{9.4}$$

[1]The invariant mass is a measure of the total energy of a system of particles that is independent of the reference frame.

Here, K is a constant depending on the total number of decays observed, W_r is the position of the maximum, and Γ is the *decay width*[2].

From the energy-time uncertainty principle[3], we have:

$$\Delta W = \Delta E \approx \Gamma \equiv \frac{1}{\tau} \tag{9.5}$$

Figure 9.3 illustrates the Breit-Wigner distribution.

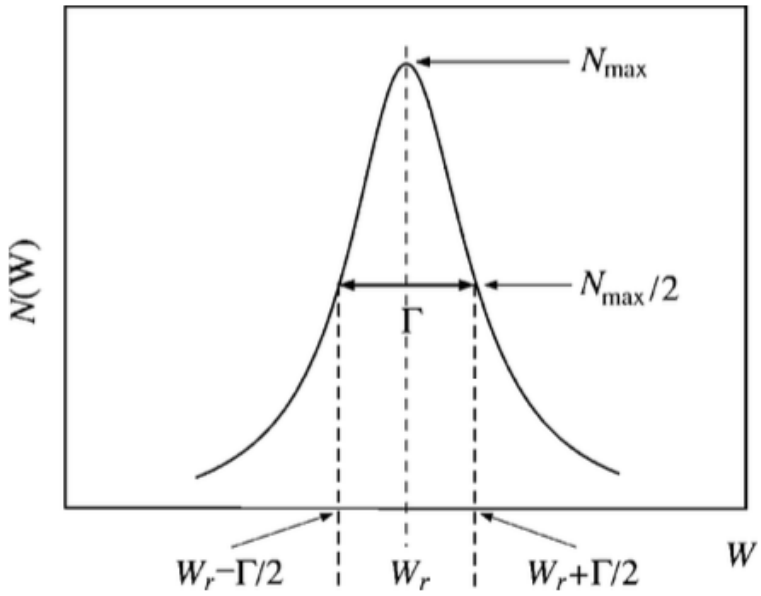

Figure 9.3: Plot of the Breit-Wigner formula.

Applying the values from Figure 9.2 to the Breit-Wigner formula, we obtain a decay width Γ of approximately 50 MeV.

[2]The decay width Γ represents the range of possible values for the energy of resonance and is related to its lifetime.

[3]The energy-time uncertainty principle states that the uncertainty in energy ΔE and the uncertainty in time Δt are inversely related: $\Delta E \cdot \Delta t \geq \hbar/2$.

Experimental Methods

Before proceeding with the chapter, we must introduce some terminology to the reader, which will clarify certain concepts as we advance.

Luminosity (L): It is defined as the ratio of the number of events detected (*dN*) in a certain period of time (*dt*) to the cross-section (σ)[1]:

$$L = \frac{1}{\sigma}\frac{dN}{dt} \tag{10.1}$$

It has dimensions of **events per time per area**. Here are a few examples of the luminosity of various accelerators.

Table 10.1: Luminosity of Current and Future Colliders

(a) Current Colliders

Collider	**Interaction**	**L ($cm^{-2}s^{-1}$)**
VEPP-2000	$e^+ + e^-$	10^{31}
SuperKEKB	$e^+ + e^-$	3×10^{34}
LHC	$p + p$	2.1×10^{34}
RHIC	$p + p$	2×10^{32}

(b) Future Colliders

Collider	**Interaction**	**L ($cm^{-2}s^{-1}$)**
CEPC	$e^+ + e^-$	2.0×10^{34}
FCC-hh	$p + p$	5.0×10^{34}
ILC	$e^+ + e^-$	10^{34}
Muon Collider	$\mu^+ + \mu^-$	10^{34}

Center of Mass Energy (E_{CM}): The center of mass frame is the reference frame in which the total momentum of the particles is zero. The center of mass energy is the total energy of the particles in this frame.

Having introduced these concepts, we can now proceed to discuss the two different types of collisions.

Fixed-Target Experiments: In these experiments, a beam is produced and directed towards a target that is stationary to the incident beam. The resulting collision will produce new particles, as illustrated in Figure 10.1.

In fixed-target experiments, the center-of-mass energy E_{CM} increases as the square root of the laboratory en-

[1]The cross-section σ is a measure of the probability that a particular process will occur when particles collide. It has units of area and gives an indication of the size of the target in a particle interaction.

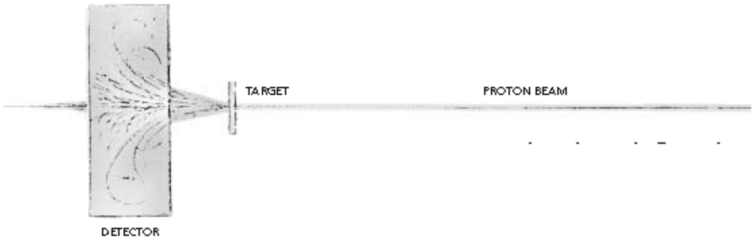

Figure 10.1: Fixed-Target Collision

ergy E_L, $E_{CM} \propto E_L^{1/2}$. This relationship imposes a significant limitation on achieving high center-of-mass energies in fixed-target setups[2].

Colliding-Beam Experiments: Two beams are produced and directed toward each other, resulting in a collision, as illustrated in Figure 10.2.

Unlike the fixed-target method, this approach exhibits a linear proportionality between the center-of-mass energy and the laboratory frame energy, $E_{CM} \propto E_L$. This linear relationship makes it easier to achieve higher center-of-mass energies, which is crucial for the study of high-energy physics.

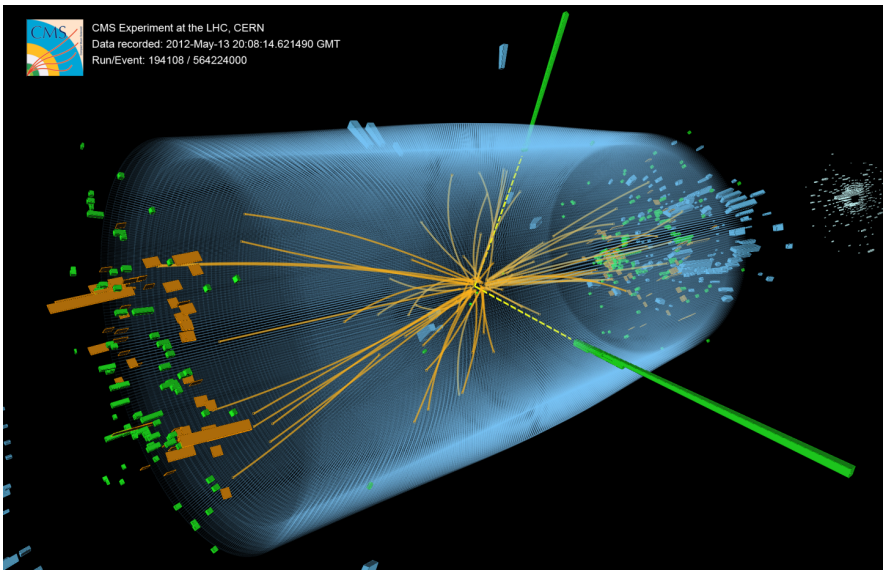

Figure 10.2: Colliding-Beam Experiments

Colliding-beam experiments also have disadvantages. The need for stable colliding particles limits the interactions studied. The collision rate is lower than in fixed-target experiments due to lower particle densities. An accelerator's performance is characterized by its luminosity L, determining the reaction rate for a given cross-section. Particles produced are analyzed through interactions with detectors placed near the interaction region. Various detectors are used, each with specific characteristics, and modern experiments typically employ multiple types.

[2]Center-of-mass energy is critical in particle physics because it determines the energy available for particle production in collisions. Higher center-of-mass energy means the potential to produce more massive particles.

10.1 Accelerators and Beams

Accelerators use electromagnetic forces to boost the energy of stable charged particles, injected from sources like electron guns or proton ion sources. They utilize radio frequency (r.f.) electric fields for acceleration and are categorized into linear and cyclic types.

10.1.1 Linear Accelerators

Proton Linacs: Protons pass through metal drift tubes in a vacuum vessel connected to alternating terminals of an r.f. oscillator (Figure 10.3). The particles are accelerated in bunches, with drift tube lengths increasing to maintain acceleration. Proton linacs often serve as injectors for synchrotrons.

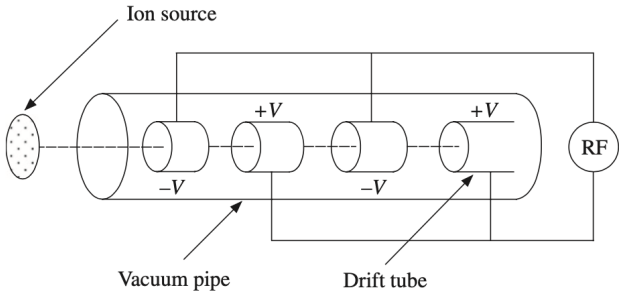

Figure 10.3: Linear Accelerator

Electron Linacs: These use cylindrical metal cavities and power from klystrons[3] to create an oscillating electric field and a magnetic field for beam focusing. The SLC at SLAC Laboratory achieves 50 GeV over 3 km with 80,000 copper cavities.

CEBAF Approach: The Continuous Electron Beam Accelerator Facility (CEBAF) uses two shorter linacs, cycling the beam to achieve energies between 0.5 and 6.0 GeV. This method reduces linac length while maintaining high beam intensity, crucial for nucleon structure studies.

10.1.2 Cyclic Accelerators

Cyclic accelerators, such as synchrotrons, use a near-circular orbit to accelerate particles. The particle beam travels in an evacuated tube called the beam pipe, guided by dipole magnets (Figure 10.4(a)) known as bending magnets.

Acceleration Process

Acceleration occurs as the beam traverses cavities where energy is supplied. Particles emit synchrotron radiation, resulting in energy loss proportional to the fourth power of their mass.

[3] Klystrons are specialized vacuum tubes that amplify high-frequency radio waves to generate the high-power microwaves necessary for accelerating particles.

$$\Delta E = \frac{4\pi q^2 \beta^3 \gamma^4}{3\epsilon_0 \rho}, \tag{10.2}$$

where $\beta = v/c$, $\gamma = (1-\beta^2)^{-1/2}$, and q is the particle's charge[4].

Momentum and Magnetic Field

The momentum of an orbiting particle is given by:

$$p = 0.3B\rho, \tag{10.3}$$

where B is the magnetic field and ρ is the radius of curvature. High-energy accelerators, such as the Large Hadron Collider (LHC) at CERN, achieve high energies by using large radii and strong magnetic fields.

Stability of the Beam

During acceleration, a beam may make many traversals of its orbit before reaching maximum energy. Stability is crucial to ensure particles remain on track and do not collide with the vacuum tube walls. Particles are accelerated in bunches, synchronized with the r.f. field. In equilibrium, a particle's momentum increases just enough to maintain a constant radius of curvature as B increases.

Focusing the Beam

Particles in the beam oscillate around stable orbits due to focusing magnets (Figure 10.4(b)), which act like optical lenses. The beam's intensity is essential for interactions, but it is limited by de-focusing effects[5] such as mutual repulsion within the beam.

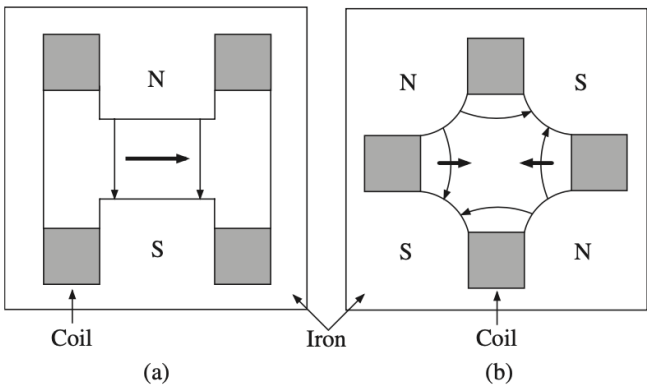

Figure 10.4: Cross-section of a typical bending (dipole) magnet (left diagram) and a focusing (quadrupole) magnet (right diagram).

[4] Synchrotron radiation is the loss of energy by charged particles when they are accelerated radially.

[5] De-focusing effects in particle beams occur when forces, such as mutual repulsion between similarly charged particles, cause the beam to spread out, reducing its intensity and focus.

High-Intensity Beams

High-intensity beams are needed for plentiful interactions, but technical challenges like de-focusing effects and particle repulsion must be addressed.

10.1.3 Fixed-Target Machines and Colliders

Accelerators can be categorized into fixed-target and colliding-beam machines. Colliders are sometimes referred to as storage rings.

Fixed-Target Machines

In fixed-target machines, particles are accelerated to high energies and directed at a stationary target, typically a solid or liquid. Higher energies have been achieved for protons than electrons due to radiation losses in electron machines. The intensity of the beam allows for a large number of interactions, useful for producing secondary beams.

The main disadvantage is the need to achieve high center-of-mass energies to produce new particles, making most modern machines colliders.

Colliders

Colliders accelerate particles to the highest energies before colliding them. The LHC at CERN is the largest operational collider, with a circumference of 27 km, a design luminosity of $L = 10^{34}\text{cm}^{-2}\text{s}^{-1}$, and beam energies of 7 TeV. The acceleration process begins with a linac, boosting the beam in the PSB (Proton Synchrotron Booster), and then to the PS (Proton Synchrotron) and SPS (Super Proton Synchrotron) before reaching the LHC. Four beam intersection points (ALICE, CMS, LHC-b, and ATLAS) facilitate various experiments.

A neutrino beam extracted at the bottom of the diagram is sent to the Gran Sasso Laboratory 750 km away for neutrino experiments.

10.1.4 Neutral and Unstable Particle Beams

Accelerators typically use stable, charged particles, but experiments also involve neutral and unstable particles like photons, neutrons, and charged pions. These beams can be produced in several ways.

10.1.5 Production of Unstable Particle Beams

Unstable particles can form beams if they travel long enough to be analyzed. One method is to direct a primary beam onto a heavy target, producing many new particles that can be separated into secondary beams of specific momentum.

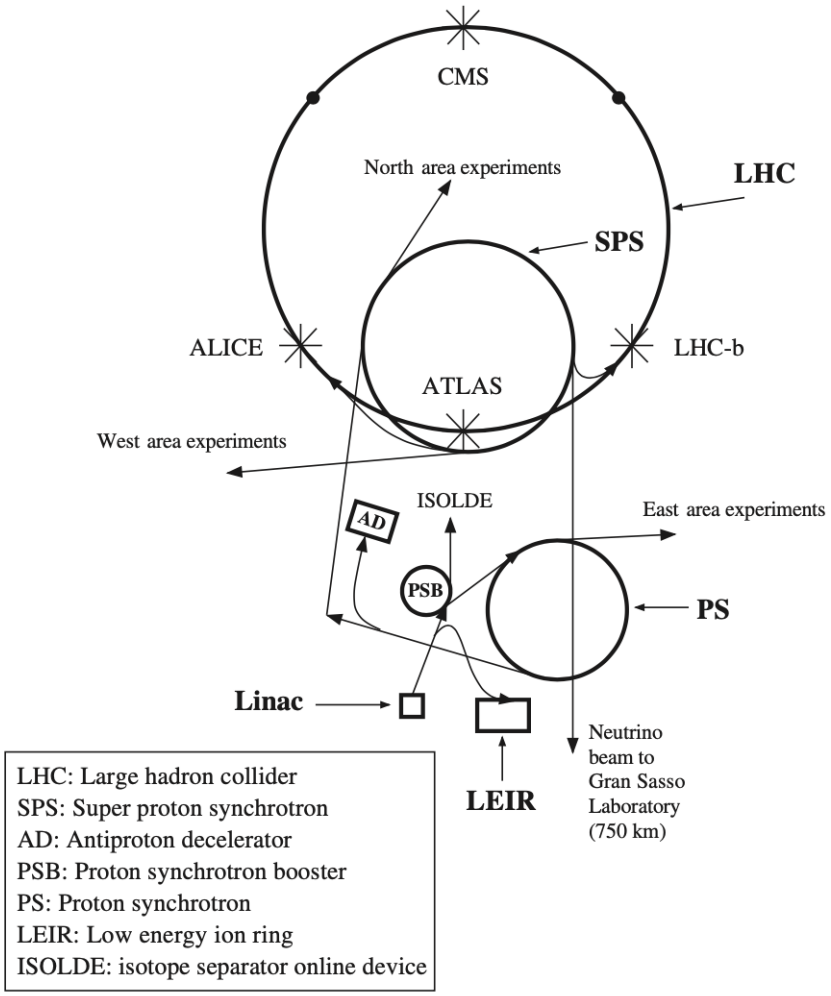

Figure 10.5: Schematic diagram of the LHC and its accelerators.

Example: π^+ Beam

A π^+ beam can be produced from a primary proton beam interacting with a heavy target, generating secondary particles, mainly pions. A collimator selects particles in a specific direction, and electrostatic fields with bending and focusing magnets create a mono-energetic π^+ beam.

Example: Neutrino Beam

A π^- beam can produce a neutrino beam. As π^- decays dominantly into μ^- and $\bar{\nu}_\mu$, passing the π^- beam through a long vacuum pipe causes many to decay, creating muons and antineutrinos. A long absorber removes muons and remaining pions, leaving neutrinos. The final neutrino beam is not monoenergetic but reflects the initial momentum spectrum of the pions. Further momentum selection using magnets is not possible as neutrinos are neutral[6].

[6]Neutrinos are neutral particles that interact very weakly with matter, making them challenging to detect and analyze.

10.2 Particle Interactions with Matter

10.2.1 Short-Range Interactions with Nuclei

For hadrons, the most significant short-range interactions with nuclei are due to the strong nuclear force. This force is crucial for both neutral and charged particles. For the simplest nucleus, the proton, the resulting reactions are of two types: elastic scattering and inelastic reactions.

Elastic scattering is represented by:

$$\pi^- + p \rightarrow \pi^- + p \tag{10.4}$$

Inelastic reactions include processes such as:

$$\pi^- + p \rightarrow \pi^+ + \pi^- + \pi^0 + n \tag{10.5}$$

$$\pi^- + p \rightarrow K^0 + \Lambda \tag{10.6}$$

The total cross-section (σ_{tot}) is the sum of the cross-section for elastic scattering (σ_{el}) and that for inelastic reactions (σ_{inel}):

$$\sigma_{\text{tot}} = \sigma_{\text{el}} + \sigma_{\text{inel}} \tag{10.7}$$

The behaviors of the total and elastic cross-sections for $\pi^- p$ scattering as functions of the pion laboratory momentum are shown in Figure 10.6.

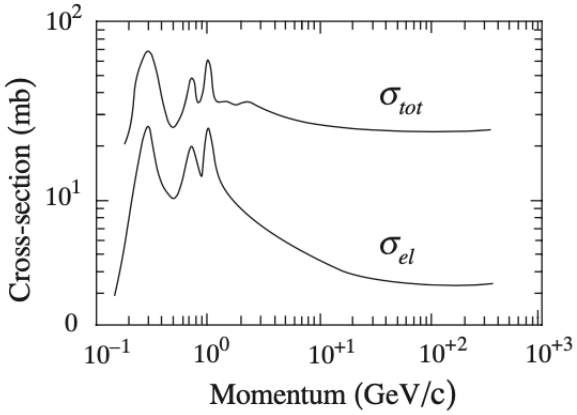

Figure 10.6: Total and elastic cross-sections for $\pi^- p$ scattering as functions of the pion laboratory momentum.

The collision length (l_c) and absorption length (l_a) are important quantities for understanding particle interactions in matter. They are defined as follows:

$$l_c = \frac{1}{n\sigma_{\text{tot}}} \tag{10.8}$$

$$l_a = \frac{1}{n\sigma_{\text{inel}}} \tag{10.9}$$

where n is the number of nuclei per unit volume. Table 10.2 summarizes the nuclear cross-sections and associated interaction lengths for various elements.

Table 10.2: Nuclear cross-sections and the associated collision lengths l_c and absorption lengths l_a for incident neutrons with energies in the range 80-300 GeV.

Element	Z	σ_{tot} (b)	l_c (cm)	l_a (cm)
H*	1	0.039	687	806
C	6	0.331	26.6	38.1
Al	13	0.634	26.1	39.4
Fe	26	1.120	10.5	16.8
Pb	82	2.960	10.2	17.1

10.2.2 Ionization Energy Losses: Bethe-Bloch Equation

Ionization energy losses are significant for all charged particles as they traverse through matter, with these losses dominating at lower and intermediate energies. The Bethe-Bloch equation describes the ionization energy loss $\left(-\frac{dE}{dx}\right)$ for a charged particle due to Coulomb scattering from atomic electrons[7].

$$-\frac{dE}{dx} = \frac{Dq^2 n_e}{\beta^2}\left[\ln\left(\frac{2m_e c^2\beta^2\gamma^2}{I}\right) - \beta^2 - \frac{\delta(\gamma)}{2}\right] \tag{10.10}$$

- D is a constant,
- q is the charge of the incident particle,
- n_e is the electron density of the medium,
- m_e is the electron mass,
- c is the speed of light,
- γ is the Lorentz factor,
- I is the mean excitation potential of the medium,
- $\delta(\gamma)$ is a correction factor for density effect.

The ionization loss rate falls rapidly as the velocity increases from zero due to the $1/\beta^2$ factor, reaching a minimum (the region of 'minimum ionization') for $\beta\gamma$ in the range 3 to 4. Beyond this range, β tends to unity, and the logarithmic factor gives a 'relativistic rise'[8].

[7] Coulomb scattering refers to the interaction between charged particles and the electric field of atomic nuclei or electrons. In the context of ionization energy loss, it describes the deflection and energy transfer that occurs when a charged particle passes close to an atomic electron.

[8] The Bethe-Bloch equation describes how charged particles lose energy when they travel through a medium by ionizing atoms. The loss rate decreases initially with increasing velocity but rises again when particles reach relativistic speeds.

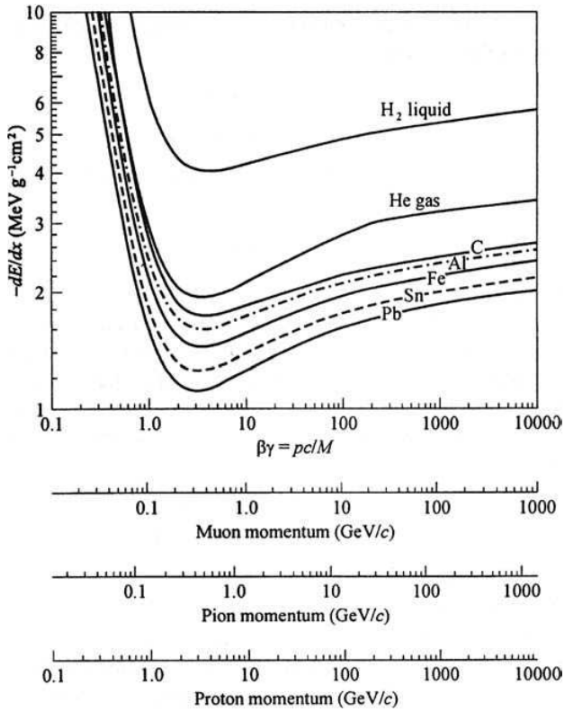

Figure 10.7: Ionization energy loss as a function of $\beta\gamma = p/Mc$ for different materials.

Typical values for minimum ionization energy loss for various materials are summarized in Table 10.3.

Table 10.3: The minimum ionization energy losses $\left(-\frac{dE}{dx}\right)_{\text{min}}$ for various materials and their dependence on the density ρ in g cm^{-3}.

Element	Z	$\left(-\frac{dE}{dx}\right)_{\text{min}}$ (MeV cm^2/g)	$\frac{1}{\rho}\left(-\frac{dE}{dx}\right)_{\text{min}}$ (MeV g cm^2)
H*	1	0.063	4.12
C	6	2.26	1.78
Al	13	2.70	1.62
Fe	26	7.87	1.48
Pb	82	11.35	1.13

10.2.3 Radiation Energy Losses

Charged particles can also lose energy through radiative collisions, especially when interacting with nuclei. These interactions cause the particles to radiate photons and lose energy. This type of energy loss is particularly significant for relativistic electrons.

The rate of energy loss due to radiation for relativistic electrons is given by:

$$-\frac{dE}{dx} = \frac{E}{L_R} \tag{10.11}$$

where L_R is the radiation length, which represents the mean distance over which a high-energy electron loses all but $1/e$ of its energy by radiation[9].

[9]Radiation length is a measure of how far a high-energy electron or photon can travel through a material before losing significant energy

The radiation length L_R is given by:

$$\frac{1}{L_R} = 4\left(\frac{\hbar}{mc}\right)^2 Z(Z+1)\alpha^3 n_a \ln\left(\frac{183}{Z^{1/3}}\right) \tag{10.12}$$

- $\hbar$ is the reduced Planck constant,
- m is the electron mass,
- c is the speed of light,
- Z is the atomic number of the material,
- α is the fine-structure constant,
- n_a is the number density of atoms in the material.

Element	Z	L_R (cm)	E_C (MeV)
H_2*	1	≈ 1000	340
C	6	18.8	103
Al	13	8.9	47
Fe	26	1.8	24
Pb	82	0.56	7

Table 10.4: The radiation length L_R and the energy E_C at which electron radiation energy losses equal their ionization energy losses for various elements.

From these results, we see that at high energies, the radiation losses are proportional to E/m_p^2 for an arbitrarily charged particle of mass m_p. On the other hand, the ionization energy losses are only weakly dependent on the projectile mass and energy at very high energies. Consequently, radiation losses completely dominate the energy losses for electrons and positrons at high enough energies, but are much smaller than ionization losses for all particles other than electrons and positrons at all but the highest energies.

10.2.4 Ranges and Interaction Lengths

The range and interaction length of particles are critical factors in determining their penetrative power in various materials. For non-relativistic charged particles ($\beta = 1$), ionization energy losses are very high, causing the particles to come to rest relatively quickly. However, for highly relativistic particles, the situation changes, and a relatively simple picture emerges for any given material.

Electrons and Photons: For energies above 1 GeV, electrons and photons are the least penetrating particles. Their interactions are controlled by the radiation lengths listed in Table 10.4.

Hadrons: For hadrons, radiation energy losses are not significant compared to electrons. Their strong interactions with atomic nuclei are controlled by the interaction lengths, which are typically much larger than the radiation lengths for electrons in the same material.

through radiation. It is crucial for understanding the behavior of particles in detectors.

Muons: Radiation energy losses for muons are surpassed by the square of their mass compared to electrons. Muons have no strong interactions with nuclei, making them the most penetrating of all charged particles.

Neutrinos: Neutrinos only interact through weak interactions, allowing them to pass through enormous distances of matter without interacting.

10.3 Gas Detectors

Gas detectors work by detecting ionization caused by charged particles passing through a gas like argon. They collect ionization products on electrodes, resulting in a pulse at the anode, which is then amplified. Typically, producing an electron-ion pair requires 30 ± 10 eV, varying slightly with the gas type and particle energy.

These detectors are often used for precise particle position measurements within a certain voltage range, known as the 'proportional region.' They have replaced older visual techniques like cloud chambers and bubble chambers.

Figure 10.8 shows the gas amplification factor (number of ion pairs per incident particle) versus applied voltage V for heavily ionizing particles (e.g., alpha particles) and lightly ionizing particles (e.g., electrons).

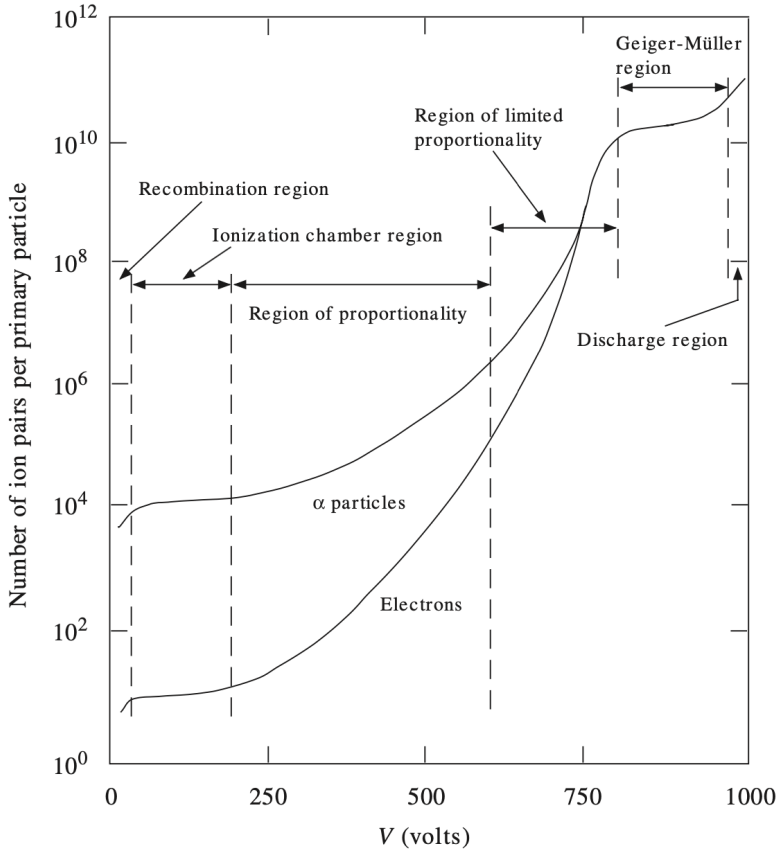

Figure 10.8: Gas amplification factor as a function of the applied voltage V for a heavily ionizing particle (upper curve) and a lightly ionizing particle (lower curve).

10.3.1 Ionization Chamber

At low voltages, electron-ion pairs recombine, resulting in a minimal output signal. As voltage increases, ion pairs reach saturation, defining the ionization chamber region. The basic setup is a parallel plate condenser with an inert gas, generating an electric field $E = \frac{V}{d}$, where d is the plate distance.

A cylindrical design uses an inner anode (r_a) and an outer cathode (r_c), creating an electric field:

$$E(r) = \frac{V}{r \ln(r_c/r_a)} \tag{10.13}$$

The signal, proportional to the ion number, is small and needs amplification. Ionization chambers have limited energy and time resolution but are useful as beam monitors in high particle flux environments.

10.3.2 Wire Chambers

When the voltage in an ionization chamber is increased beyond the ionization region, the chamber enters the proportional region. In this region, the electric field strengths near the wire can reach $10^4 - 10^5$ V/cm, which is strong enough for the electrons from the initial ionization to gain sufficient energy to cause secondary ionizations, resulting in a rapid amplification known as the Townsend avalanche[10]. The output signal at the anode remains proportional to the energy lost by the original particle.

Devices operating in this proportional region are known as track chambers or simply wire chambers. One of the earliest implementations of this idea was the proportional counter, a cylindrical tube filled with gas containing a quenching component.

A significant advancement in proportional counters was the development of the multiwire proportional chamber (MWPC), introduced in 1968. The MWPC features multiple anode wires arranged in a plane between cathode plates, each wire acting as an independent detector. MWPCs achieve high spatial resolution (50-200 μm) and a typical time resolution of about 2 ns.

10.3.3 Drift Chambers

Drift chambers, which have largely replaced MWPCs, use the time it takes for liberated electrons to drift from their point of production to the anode to measure the passage of charged particles. The delay between the passage of a particle and the creation of a pulse at the anode correlates with the particle's trajectory and the anode wire. Additional wires provide a consistent electric field, and a reference time is set by a scintillator[11].

Drift chambers are versatile and available in planar, radial, or cylindrical configurations. For instance, the JADE collaboration at the DESY collider used a cylindrical array of drift chambers to study e^+e^- interactions. These chambers allowed for the reconstruction of charged particle trajectories considering the known magnetic

[10] The Townsend avalanche is a process in which free electrons gain enough energy from the electric field to ionize additional gas molecules, creating a cascade of ionization. This phenomenon is crucial for the functioning of gas detectors.

[11] A scintillator is a material that emits light when it is excited by ionizing radiation. They convert this energy into light, which can then be detected by photodetectors.

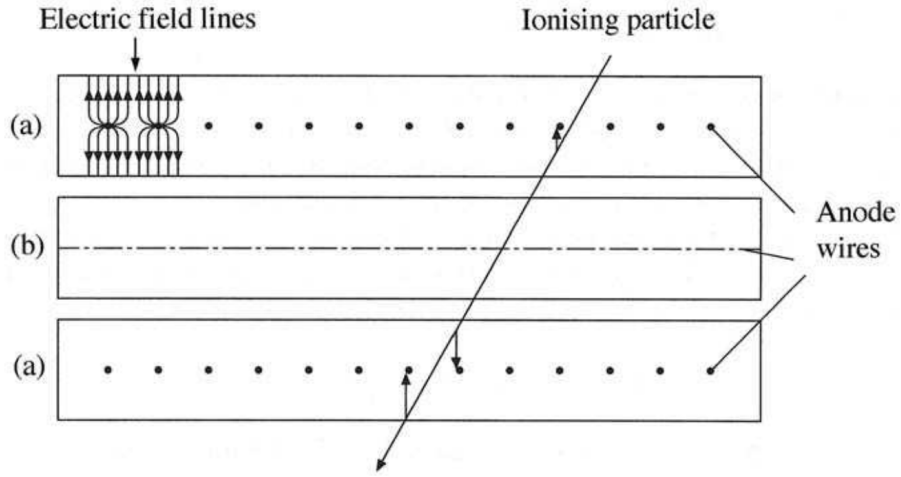

Figure 10.9: A group of three planes of an MWPC. Planes (a) have anode wires into the page, and those in the plane (b) are at right angles.

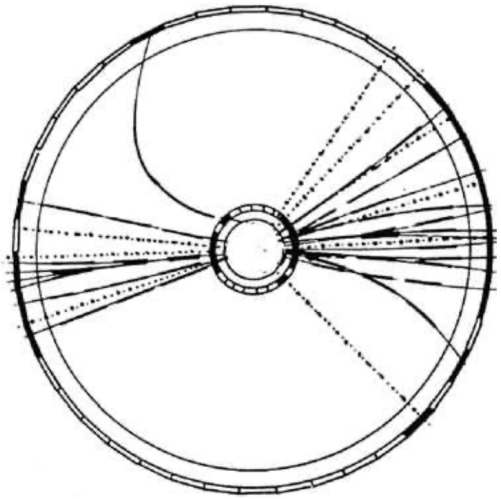

Figure 10.10: Computer reconstruction of a typical 'two-jet' event in a drift chamber. Solid lines are trajectories of charged particles, and dotted lines are neutral particles.

field.

10.3.4 Time Projection Chambers (TPC)

The Time Projection Chamber (TPC) represents an advanced application of proportional and drift chamber principles. The TPC consists of a cylindrical barrel surrounding the beam pipe of a collider. A high-voltage electrode plane at the center of the chamber generates an electric drift field, while a strong magnetic field aligns parallel and antiparallel to the cylinder axis.

Electrons formed along the track of an ionizing particle drift under the electric field towards the endcap wire chambers. The time taken for electrons to drift from production to the endcaps provides the third coordinate necessary for reconstructing the particle's position.

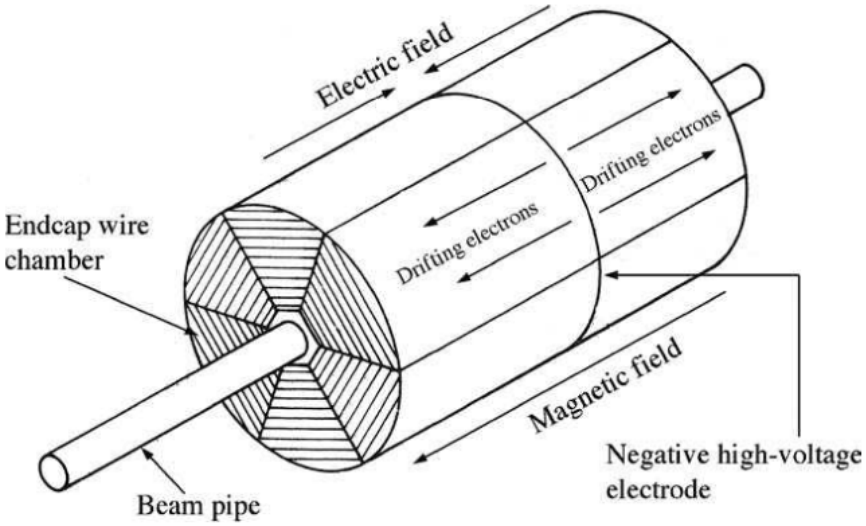

Figure 10.11: Schematic diagram of a Time Projection Chamber (TPC).

A more robust evolution of the chamber is the microstrip gas chamber (MSGC), which replaces wires with conductive metal strips on a printed circuit board. The MSGC is used in modern large accelerators for its durability and precision.

10.3.5 Beyond the Region of Proportionality

Referencing Figure 10.8, increasing the external voltage further moves us into the *limited proportionality* region, where the output signal is no longer proportional to the ion pairs produced. Beyond this, we reach the *Geiger-Müller region*, where the signal is independent of the incident energy. Detectors in this region are called *Geiger-Müller counters* and are commonly used in portable radiation monitors.

If the voltage is increased even more, the gas amplification creates moving plasmas or streamers, leading to visible light and electrical output. Eventually, a complete breakdown occurs, emitting a spark. Detectors in this high-voltage region, known as *streamer and spark chambers*, were widely used in the 1970s and 1980s for hadron physics but are now largely obsolete.

10.4 Semiconductor Detectors

Semiconductor detectors operate by promoting electrons from the valence band to the conduction band when a charged particle passes through. The absence of an electron creates a 'hole,' and the electron-hole pairs are proportional to the energy loss. An external electric field separates these pairs, producing a signal.

Typically made from silicon, these detectors have a small band gap (1 eV) and low energy loss to produce pairs (3-4 eV), making them effective for detecting low-energy particles. They offer excellent energy resolution and fast response times[12]. Silicon microstrip detectors, with 10 μm gaps, and pixel detectors are common types,

[12]Semiconductor detectors, like silicon detectors, are highly efficient for particle detection due to their ability to produce electron-hole

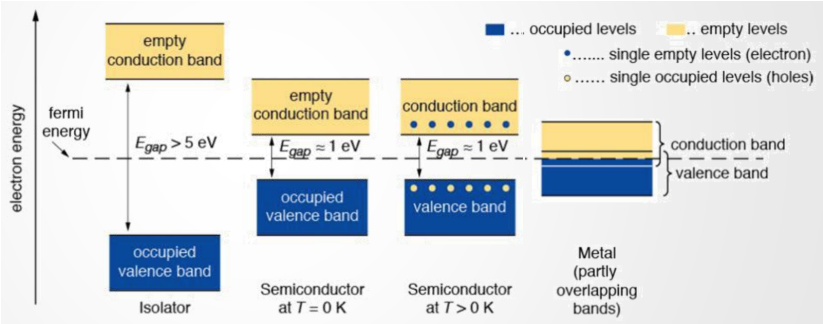

Figure 10.12: Energy band diagrams for an insulator, a semiconductor at $T = 0$ K and $T > 0$ K, and a metal.

providing high spatial resolution. These detectors are crucial in particle physics experiments at colliders like the LHC but are limited by radiation damage.

10.5 Scintillation Counters

Scintillation counters detect charged particles by using materials called scintillators, which emit light when excited by ionization or excitation. This light is directed to a photodetector, which converts the light into an electrical signal. Often, a wavelength shifter[13] adjusts the light to match the photodetector's sensitivity.

Photomultiplier Tube: A photomultiplier tube (PMT) is a common photodetector that amplifies the light signal. It emits electrons from a cathode, which are then amplified by a series of dynodes, resulting in a measurable electric signal.

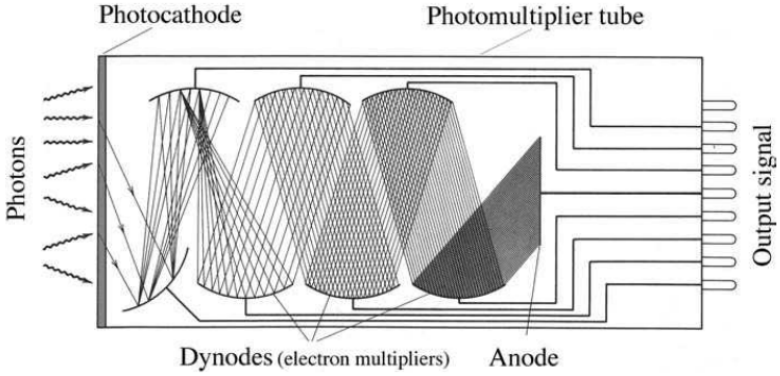

Figure 10.13: Schematic diagram of the main elements of a photomultiplier tube.

Applications: Scintillation counters are ideal for timing and triggering other detectors. They can also distinguish between particles by measuring the time-of-flight between two counters. However, they are limited to low-energy particles since high-energy particles travel near the speed of light.

pairs with minimal energy loss. They are integral to modern particle physics experiments.

[13] A wavelength shifter is a material that absorbs light at one wavelength and re-emits it at a longer wavelength, usually to match the sensitivity range of the photodetector.

Types of Scintillators: Scintillators can be inorganic single crystals (e.g., cesium iodide) or organic liquids and plastics. Their robustness and simplicity, along with low cost and ease of fabrication, make scintillation counters essential in experimental particle physics.

10.6 Čerenkov Counters

Čerenkov counters detect high-energy particles through the Čerenkov effect. When a charged particle moves faster than the speed of light in a medium, it emits Čerenkov radiation at a characteristic angle. This radiation is detected and used to measure the particle's velocity.

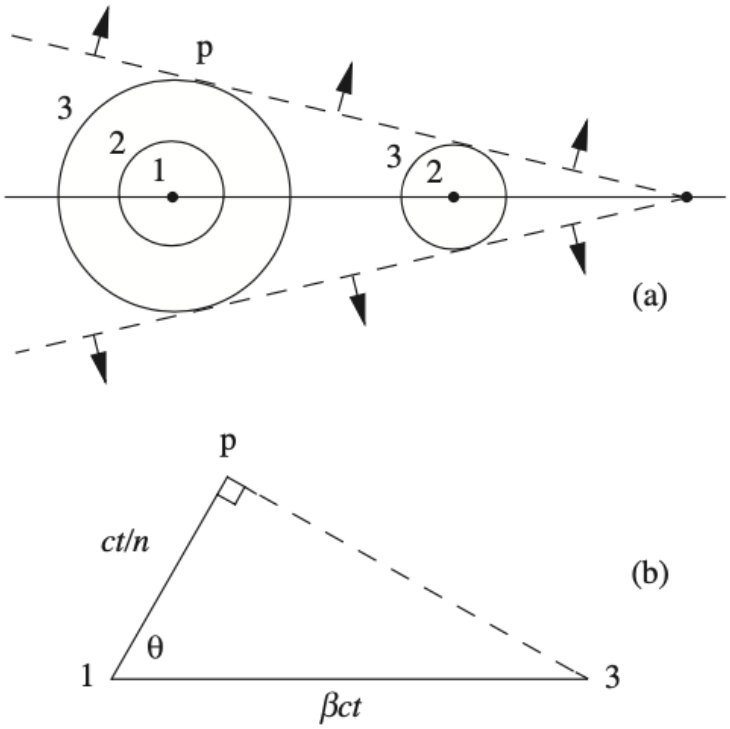

Figure 10.14: Huygen's construction for the Čerenkov radiation emitted by a particle traveling with speed v greater than c/n, the speed of light in the medium.

Application: Čerenkov radiation appears as a continuous spectrum and may be collected on a photosensitive detector. The number of photons radiated per unit path length depends on the particle's speed and the medium's refractive index.

$$N(\lambda)d\lambda = 2\pi\alpha\left(1 - \frac{1}{\beta^2 n^2}\right)\frac{d\lambda}{\lambda^2} \tag{10.14}$$

Detection Modes: Čerenkov counters can be used as threshold counters to detect particles exceeding a certain velocity or as ring-imaging detectors to measure particle velocities. The latter uses mirrors to focus Čerenkov

Table 10.5: The refractive index n and the threshold value of γ_h for various Čerenkov radiators.

Medium	$n-1$	γ_h	Photons/cm
Helium (STP)	3.5×10^{-5}	120	0.03
CO_2 (STP)	4.1×10^{-4}	35	0.40
Silica aerogel	$0.025 - 0.075$	$4.6 - 2.7$	$24 - 66$
Water	0.33	1.52	213
Glass	$0.46 - 0.75$	$1.37 - 1.22$	$261 - 331$

radiation into a ring image, allowing precise velocity measurements.

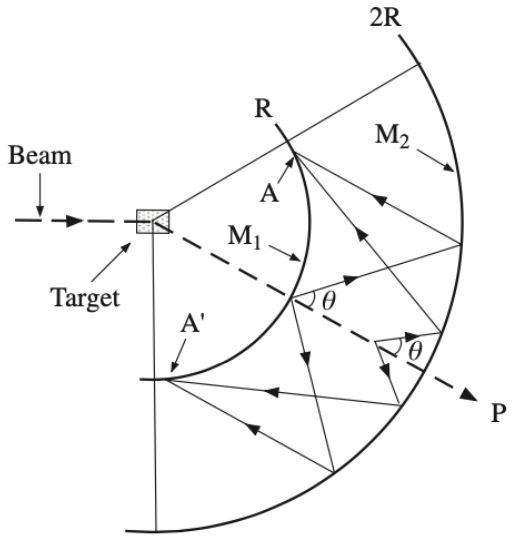

Figure 10.15: A particle P, produced from the target, emits Čerenkov radiation at an angle θ on traversing a medium contained between two spheres of radius R and $2R$.

The SuperKamiokande detector, for example, uses Čerenkov radiation to detect neutrino interactions in pure water[14].

10.7 Calorimeters

Calorimeters are special detectors that measure the energy and position of particles by absorbing them completely. Unlike other detectors, calorimeters can detect both neutral and charged particles. There are two main types of calorimeters:

- **Homogeneous Calorimeters:** These are made of a single type of material that acts as both the absorber and the detector, like a scintillator.
- **Sampling Calorimeters:** These consist of alternating layers of absorber material (like metal) and detector material (like scintillators or MWPCs).

When a particle hits the calorimeter, it interacts with the material, creating a cascade or "shower" of secondary particles. This process continues until the primary particle's energy is fully absorbed and a signal is produced

[14] SuperKamiokande is a large water Čerenkov detector located in Japan, designed to study neutrinos by observing the Čerenkov radiation they produce when interacting with water.

in the detector.

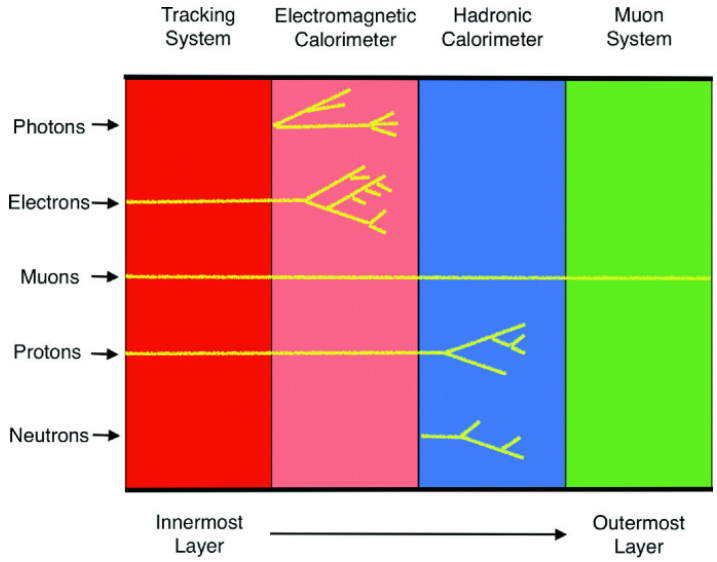

Figure 10.16: Illustration of a particle shower in a calorimeter.

Calorimeters are crucial because:

- They can detect neutral particles by observing the charged secondary particles they produce.
- The energy measurements they provide are highly precise, with accuracy improving as energy increases.
- They produce signals very quickly, which is essential for making fast decisions in experiments.

10.7.1 Electromagnetic Showers

When a high-energy electron or positron hits a calorimeter, it loses energy primarily through a process called bremsstrahlung (braking radiation). This energy loss leads to the creation of photons, which in turn produce electron-positron pairs, creating a cascade of particles.

The key steps in the shower process are:

1. An electron with energy higher than a critical value loses energy by emitting a photon.
2. Each photon, if it has enough energy, creates an electron-positron pair.
3. This cascade continues until the particles' energy falls below the critical value, where ionization losses become significant.

Here's a simplified formula that describes the energy at each stage of the shower:

$$E(t) = \frac{E_0}{2^t} \tag{10.15}$$

where E_0 is the initial energy of the electron, and t is the number of radiation lengths the particle has traveled.

The process stops when the energy of the particles reaches the critical energy E_C, and the number of particles at this point can be estimated by:

$$N_{\text{max}} = \frac{E_0}{E_C} \tag{10.16}$$

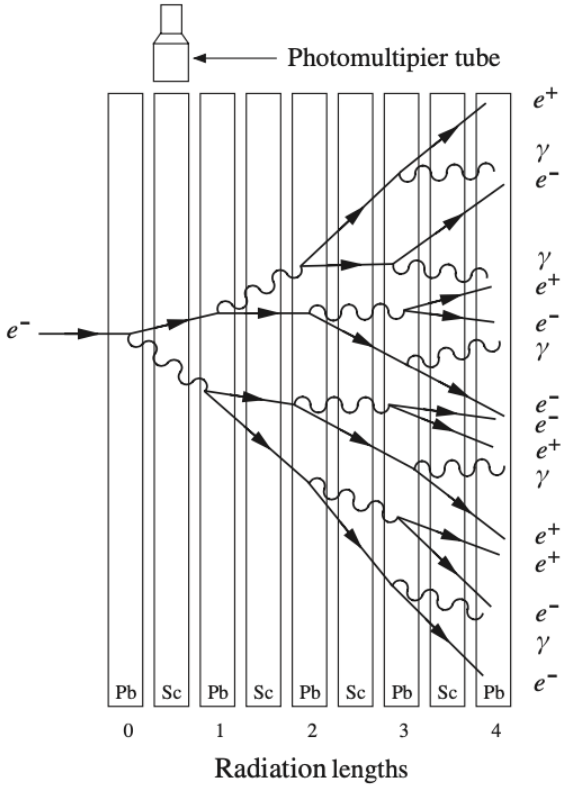

Figure 10.17: Development of an electromagnetic shower in a sampling calorimeter.

10.7.2 Hadronic Showers

Hadronic showers occur when hadrons (like protons or neutrons) interact with the calorimeter. These showers are more complex than electromagnetic ones because they involve many different processes, including the production of secondary hadrons.

Key points about hadronic showers:

- The scale of the shower is determined by the nuclear absorption length, which is larger than the radiation length for electromagnetic showers.
- Hadronic calorimeters need to be thicker because they have to absorb more energy.
- Some energy may be lost through nuclear excitation and leakage of secondary particles like muons and neutrinos, making energy measurement less precise than in electromagnetic calorimeters[15].

In summary, calorimeters are vital tools in particle physics for measuring the energy and position of particles. They can handle both charged and neutral particles and provide quick, precise energy measurements essential for high-energy physics experiments.

[15]Hadronic showers involve interactions between hadrons and nuclei, leading to the production of many secondary particles. This complexity requires thicker detectors and can result in less precise energy measurements.

Space-Time Symmetries

Symmetries and conservation laws are fundamental in physics, especially in particle physics. This chapter focuses on space-time symmetries and their role in strong and electromagnetic interactions. These conservation laws are essential in spectroscopy, helping us understand the internal structure of hadrons in terms of their constituent quarks. Each state in the spectrum has a specific energy and well-defined quantum numbers associated with conserved observables. In both atomic and hadron spectroscopy, quantum numbers are crucial for understanding energy levels, their behaviors in electric and magnetic fields, and the selection rules governing transitions. This chapter will explore the appropriate conserved quantities in hadron spectroscopy and their values for observed states. We will discuss conservation laws such as parity and charge conjugation, which are conserved in strong and electromagnetic interactions but can be violated by weak interactions. Weak interactions and their violations will be covered later. Here, we focus on the strong and electromagnetic interactions. The conservation laws originate from the symmetries and invariance properties of the underlying interactions. These principles help us understand the fundamental nature of particles and their interactions.

11.1 Classification of Particles

All particles, whether elementary (such as leptons and quarks) or composite (such as protons and neutrons), possess *quantum numbers*[1]. One significant quantum number is *spin*, denoted by S (Figure 11.1). The spin quantum number defines a particle's intrinsic angular momentum with respect to its own rest frame[2]. For composite particles, like protons which are made of three quarks, the rest frame corresponds to the center-of-mass frame of its constituents[3].

Another well-defined quantum number is the *orbital angular momentum*. The orbital angular momentum vector $\mathbf{L}$ describes the rotation of a particle around a point, similar to how the Earth orbits the Sun. Just as the Earth possesses orbital angular momentum due to its revolution around the Sun and spin angular momentum due to its rotation on its axis, particles also exhibit these forms of angular momentum. The vector $\mathbf{L}$ combines both

[1] Quantum numbers are values that describe specific properties of particles, such as charge, spin, and angular momentum.
[2] The rest frame of a particle is a reference frame in which the particle is at rest.
[3] The center-of-mass frame is a reference frame where the total momentum of a system is zero.

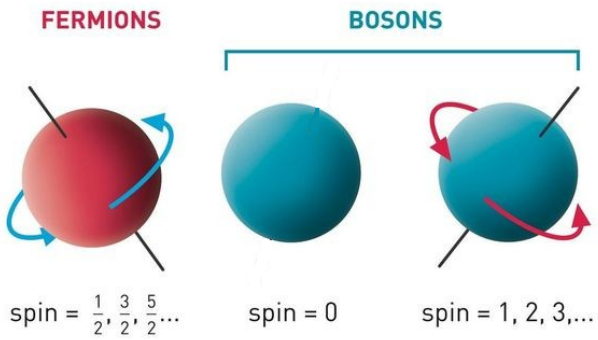

Figure 11.1: Spins of different particles

the direction and magnitude of the rotational motion, aiding in the understanding of the particle's rotational dynamics.

The total angular momentum of a particle, represented by *J*, is the sum of its spin and orbital angular momentum. To simplify the representation of complex electron structures and predict the chemical and physical properties of elements, we use a systematic notation called *spectroscopic notation*:

$$^{2S+1}L_J, \tag{11.1}$$

where *S* is the spin quantum number, and the total angular momentum J is given by:

$$J = |L - S|, |L - S| + 1, \ldots, L + S. \tag{11.2}$$

In this notation, the orbital angular momentum L is represented by the letters:

- $L = 0$ is denoted by *S* (sharp),
- $L = 1$ is denoted by *P* (principal),
- $L = 2$ is denoted by *D* (diffuse),
- $L = 3$ is denoted by *F* (fundamental).

These notations correspond to the shapes of the s, p, and d orbitals in atomic physics. Figure 11.2 shows these orbitals, helping to visualize how the angular momentum quantum number L relates to the spatial distribution of an electron cloud around an atom's nucleus.

This notation provides a concise and systematic way to describe the angular momentum states of particles.

Before applying these ideas to hadrons, let's consider a simple example from nuclear physics: the deuteron, which is a bound state of a neutron and a proton. In this case, we treat the nucleons as elementary spin-$\frac{1}{2}$ particles[4]. Since the deuteron has a total spin of 1, the total angular momentum J of the proton-neutron (pn) system in its center-of-mass frame is also 1.

[4]Spin-$\frac{1}{2}$ particles have intrinsic angular momentum values of $\pm\frac{1}{2}$.

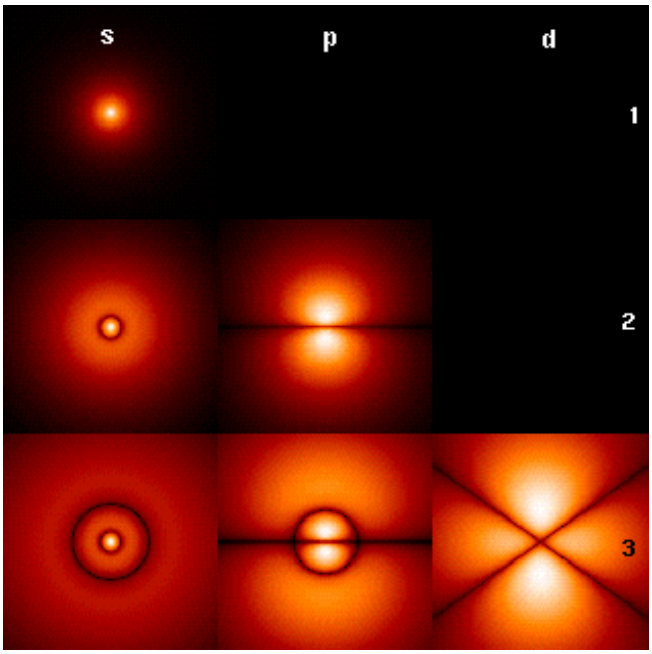

Figure 11.2: Shapes of the s, p, and d orbitals

For the lowest energy state, we assume $L = 0$ because the lowest bound states are usually S waves. Thus, $S = 1$ is the combined spin of the proton and neutron. Using spectroscopic notation, the deuteron is a ${}^{2S+1}L_J = {}^3S_1$ bound state of the pn system.

11.2 Angular Momentum in the Quark Model

In the quark model, we assume L (orbital angular momentum) and S (spin) as well-defined quantum numbers. The lightest states for any $q\bar{q}$ and $3q$ systems have zero orbital angular momentum.

Mesons are $q\bar{q}$ bound states. In the meson's rest frame, there is a single orbital angular momentum L, and two spins S_q and $S_{\bar{q}}$:

$$S = S_q + S_{\bar{q}}. \tag{11.3}$$

Both q and $\bar{q}$ have spin-$\frac{1}{2}$. For $L = 0$, $J = S$:

$${}^{2S+1}L_J = {}^1S_0, {}^3S_1 \quad (L = 0). \tag{11.4}$$

For $L \geq 1$, J values are $J = L \pm 1, L$:

$${}^{2S+1}L_J = {}^1L_L, {}^3L_{L+1}, {}^3L_L, {}^3L_{L-1} \quad (L \geq 1). \tag{11.5}$$

11.2.1 Baryons and Their Angular Momentum

Baryons are $3q$ bound states. There are two orbital angular momenta: L_{12} (between two quarks) and L_3 (third quark around the center of mass). The total orbital angular momentum L is:

$$\mathbf{L} = \mathbf{L}_{12} + \mathbf{L}_3, \tag{11.6}$$

and the total spin S is the sum of the three quarks' spins:

$$S = S_1 + S_2 + S_3, \tag{11.7}$$

giving $S = \frac{1}{2}$ or $S = \frac{3}{2}$. Baryon states in spectroscopic notation are:

$$^{2S+1}L_J = {}^2S_{1/2}, {}^4S_{3/2} \quad (L = 0), \tag{11.8}$$

$$^{2S+1}L_J = {}^2P_{1/2}, {}^2P_{3/2}, {}^4P_{1/2}, {}^4P_{3/2}, {}^4P_{5/2} \quad (L = 1), \tag{11.9}$$

$$^{2S+1}L_J = {}^2L_{L+1/2}, {}^2L_{L-1/2}, {}^4L_{L-3/2}, {}^4L_{L-1/2}, {}^4L_{L+1/2}, {}^4L_{L+3/2} \quad (L \geq 2). \tag{11.10}$$

Baryons, like protons and neutrons, have a more complex structure. The internal orbital angular momenta of a three-quark state are shown in Figure 11.3.

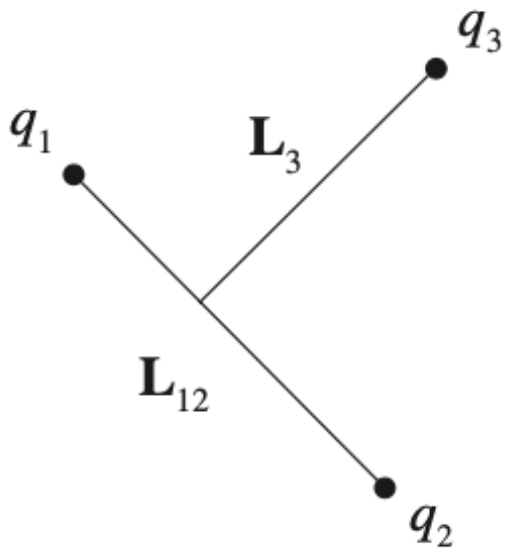

Figure 11.3: Internal orbital angular momenta of a three-quark state.

This figure illustrates how the total angular momentum $\mathbf{L}$ is composed of $\mathbf{L}_{12}$ (the orbital angular momentum of

two quarks) and $\mathbf{L}_3$ (the orbital angular momentum of the third quark). This total angular momentum combines with the spins of the quarks to form the baryon's spin.

11.3 Parity

Parity transformation involves reflecting the position vector of every particle through the origin. Mathematically, this is represented as:

$$\mathbf{r_i} \to \mathbf{r_i'} = -\mathbf{r_i}, \tag{11.11}$$

This means that the Hamiltonian[5] H of the system remains unchanged under this transformation, the system is said to be invariant under parity:

$$H(\mathbf{r_1'}, \mathbf{r_2'}, \ldots) = H(-\mathbf{r_1}, -\mathbf{r_2}, \ldots). \tag{11.12}$$

We introduce a parity operator $\hat{P}$ for a single particle (e.g., electron, muon):

$$\hat{P}\psi(\mathbf{r}, t) \equiv P_a \psi(-\mathbf{r}, t), \tag{11.13}$$

where P_a is the intrinsic parity of particle a. Since two successive parity transformations leave the system unchanged, we have:

$$\hat{P}^2\psi(\mathbf{r}, t) = \psi(\mathbf{r}, t) \implies P_a = \pm 1. \tag{11.14}$$

For a particle with a definite orbital angular momentum, the parity is given by:

$$\text{Parity} = P_a(-1)^L, \tag{11.15}$$

where L is the orbital angular momentum quantum number.

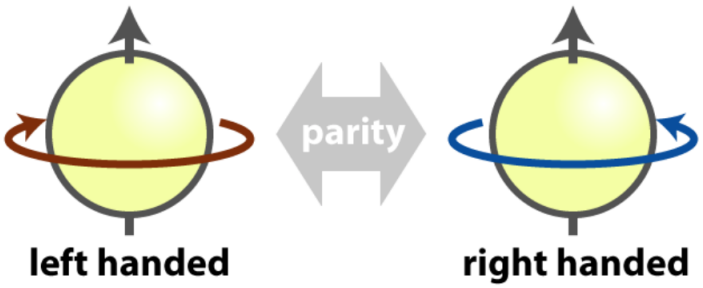

Figure 11.4: Illustration of the parity transformation and its effects on the symmetry of the particles.

[5] A Hamiltonian is a function used to describe the total energy of a system in physics. It includes both kinetic and potential energy.

This simple transformation helps us understand how the symmetry of physical systems is affected by parity and provides insight into the behavior of particles under this transformation.

11.3.1 Parity - Leptons and Quarks

Parity for leptons and quarks follows certain conventions. For leptons like electrons (e^-), muons (μ^-), and tau particles (τ^-):

$$P_{e^-} = P_{\mu^-} = P_{\tau^-} \equiv 1, \tag{11.16}$$

$$P_{e^+} = P_{\mu^+} = P_{\tau^+} \equiv -1, \tag{11.17}$$

Similarly, for quarks (u, d, s, c, b, t):

$$P_u = P_d = P_s = P_c = P_b = P_t \equiv 1, \tag{11.18}$$

$$P_{\bar{u}} = P_{\bar{d}} = P_{\bar{s}} = P_{\bar{c}} = P_{\bar{b}} = P_{\bar{t}} \equiv -1, \tag{11.19}$$

The parity of the photon (γ) is:

$$P_\gamma = -1. \tag{11.20}$$

11.3.2 Parity - Mesons and Hadrons

The intrinsic parity P_M of a meson $M = q\bar{q}$ is given by:

$$P_M = P_a P_{\bar{b}} (-1)^L = (-1)^{L+1}, \tag{11.21}$$

For baryons ($B = abc$), the parity P_B is:

$$P_B = P_a P_b P_c (-1)^{L_{12}} (-1)^{L_3} = (-1)^{L_{12}+L_3}, \tag{11.22}$$

where L_{12} and L_3 are the internal angular momenta, illustrated in Figure 11.3.

For antibaryons ($\bar{B} = \bar{a}\bar{b}\bar{c}$):

$$P_{\bar{B}} = P_{\bar{a}} P_{\bar{b}} P_{\bar{c}} (-1)^{L_{12}} (-1)^{L_3} = -(-1)^{L_{12}+L_3} = -P_B. \tag{11.23}$$

This means baryons and antibaryons have opposite parities.

11.4 Charge Conjugation

Charge conjugation is the operation that replaces all particles by their antiparticles in the same state. Charge conjugation, like parity, is conserved in electromagnetic and strong interactions.

$$\hat{C}\left|f\bar{f};J,L,S\right\rangle = (-1)^{L+S}\left|f\bar{f};J,L,S\right\rangle, \tag{11.24}$$

For a fermion-antifermion pair with total, orbital, and spin angular momentum quantum numbers J, L, and S, respectively, the charge conjugation operator acts as shown above. The C-parity of the photon is given by:

$$C_\gamma = -1. \tag{11.25}$$

Charge conjugation ($\hat{C}$) is the operation that replaces all particles by their antiparticles in the same state, so that momenta, positions, etc., are unchanged. Since the charge and magnetic moment[6] of every particle is reversed, the electromagnetic interaction remains invariant under this operation. Charge conjugation is also a symmetry of the strong interaction but is violated by the weak interaction, as we shall see in Chapter 14. Again, we shall neglect weak interactions for the present and assume invariance of the Hamiltonian and the associated conservation law:

$$[\hat{C}, H] = 0 \tag{11.26}$$

for strong and electromagnetic interactions only[7].

We now distinguish between those particles $a = \pi^+, K^+, p, N, \ldots$ that have distinct antiparticles and those particles $\alpha = \pi^0, \gamma, \ldots$ that do not. Charged particles of all types are obvious examples of the former, but some neutral particles, like the neutron which has a nonzero magnetic moment, also belong to the former category. For these particles, we have:

$$\hat{C}\left|\alpha\Psi\right\rangle = C_\alpha\left|\alpha\Psi\right\rangle^{8} \tag{11.27}$$

and

$$\hat{C}\left|\alpha\Psi\right\rangle = \left|\bar{\alpha}\Psi\right\rangle, \tag{11.28}$$

[6]The magnetic moment is a vector quantity associated with the magnetic field produced by the motion of a charged particle, such as an electron or proton, around a nucleus or through space.

[7]The commutator $[\hat{C}, H] = 0$ signifies that the charge conjugation operator $\hat{C}$ and the Hamiltonian H commute, implying that charge conjugation is a conserved symmetry in strong and electromagnetic interactions.

[8]In quantum mechanics, an eigenstate is a state of a system that does not change (except for a phase factor) when an operator is applied to it. Here, $|\alpha\Psi\rangle$ is an eigenstate of the charge conjugation operator $\hat{C}$. The corresponding eigenvalue C_α indicates the factor by which the eigenstate is scaled when the operator is applied.

where C_α is a phase factor analogous to that introduced in the discussion of parity. Since a second transformation turns antiparticles back into particles, we require $\hat{C}^2 = 1$ and hence:

$$C_\alpha = \pm 1. \tag{11.29}$$

From the above, we see that particles like $\alpha = \pi^0, \gamma, \ldots$ are eigenstates of $\hat{C}$ with eigenvalues $C_\alpha = \pm 1$, called their C-parities[9]. These values are readily measured using C conservation. For a fermion-antifermion pair with total, orbital, and spin angular momentum quantum numbers J, L, and S, we have:

$$\hat{C} \left| f\bar{f}; J, L, S \right\rangle = (-1)^{L+S} \left| f\bar{f}; J, L, S \right\rangle. \tag{11.30}$$

Thus, if the π^0, for example, is a ${}^1S_0$ state of $u\bar{u}$ or $d\bar{d}$, as assumed in the quark model, then it must have C-parity $C_{\pi^0} = 1$.

11.4.1 Neutral Pion Decay

Neutral pions (π^0) are composed of quark-antiquark pairs $u\bar{u}$ or $d\bar{d}$. For the neutral pion, the state ${}^{2S+1}L_J$ is ${}^1S_0$.

The C-parity of the neutral pion π^0 is given by:

$$C_{\pi^0} = (-1)^{L+S} \tag{11.31}$$

For π^0, $L = 0$ and $S = 0$, so:

$$C_{\pi^0} = (-1)^{0+0} = 1 \tag{11.32}$$

The neutral pion decays into two photons:

$$\pi^0 \to \gamma + \gamma \tag{11.33}$$

Using charge conjugation for photons, we have:

$$\hat{C}|\gamma\gamma\rangle = C_\gamma C_\gamma |\gamma\gamma\rangle = |\gamma\gamma\rangle \tag{11.34}$$

For photons, $C_\gamma = -1$, so:

$$C_{\gamma\gamma} = (-1) \times (-1) = 1 \tag{11.35}$$

[9]C-parity is a property of certain particles, indicating how their wavefunction changes under the charge conjugation operation.

Thus, the C-parity of the π^0 decay into two photons is consistent with $C_{\pi^0} = 1$.

11.4.2 Eta Decay

The eta (η) is a neutral spin-0 meson. It decays into multiple final states. Let's analyze these decays step-by-step:

$$\eta \to \gamma + \gamma, \quad B = 0.3943 \pm 0.0020 \tag{11.36}$$

This decay is electromagnetic (EM) as it involves photons.

$$\eta \to \pi^0 + \pi^0 + \pi^0, \quad B = 0.3269 \pm 0.0026 \tag{11.37}$$

$$\eta \to \pi^+ + \pi^- + \pi^0, \quad B = 0.2292 \pm 0.0028 \tag{11.38}$$

Given that the first decay is electromagnetic, and the other two decays have comparable rates, it is reasonable to assume they are also electromagnetic. The C-parity of the eta meson can be inferred from these decays as again 1.

The Quark Model

The quark model is essential for understanding hadrons, particles composed of quarks bound by a strong force. In this framework, baryons consist of three quarks, while mesons are quark-antiquark pairs. A critical feature is *isospin symmetry*, where the strong force is independent of quark flavor, making interactions like ud and us identical[1]. To resolve the apparent violation of the Pauli Exclusion Principle[2], the quark model introduces *color charge*, ensuring quarks can exist together within particles like the Δ^{++} baryon (uuu) without conflict. Quark confinement, the principle that quarks cannot exist independently, ensures they remain within hadrons. At the same time, a system like charmonium ($c\bar{c}$) is studied for its energy level in a nonrelativistic context[3].

12.1 Isospin Symmetry

Isospin symmetry is a key concept in the classification of hadrons, allowing them to be grouped into families with similar properties. This symmetry reflects the near equivalence of the strong forces acting on up (u) and down (d) quarks, leading to particles such as the proton (p) and neutron (n) being part of the same isospin multiplet[4].

For example, consider the nucleons:

$$p(938) = uud, \quad n(940) = udd, \tag{12.1}$$

and the K mesons:

$$K^+(494) = u\bar{s}, \quad K^0(498) = d\bar{s}. \tag{12.2}$$

These particles are part of isospin multiplets, where the symmetry would be perfect if the masses of u and d quarks were exactly equal[5].

[1] Isospin symmetry simplifies the study of hadrons by treating different quark flavors similarly.
[2] The Pauli Exclusion Principle states that no two identical fermions can occupy the same quantum state.
[3] These systems allow for precise calculations using the Schrödinger equation.
[4] Isospin symmetry simplifies the analysis of hadrons by treating different quark flavors similarly.
[5] In reality, the d quark is slightly more massive than the u quark by a few MeV/c^2, primarily due to electromagnetic interactions.

12.1.1 Isospin Quantum Numbers

To describe isospin symmetry more precisely, we introduce specific quantum numbers. The first is the hypercharge (Y), defined as:

$$Y = B + S + C + \tilde{B} + T, \tag{12.3}$$

where B is the baryon number, S is strangeness, C is charm, $\tilde{B}$ is bottomness, and T is topness.

The third component of isospin, I_3, is given by:

$$I_3 \equiv Q - \frac{Y}{2}, \tag{12.4}$$

alternatively, in terms of the quark content:

$$I_3 = \frac{1}{2}(N_u - N_d), \tag{12.5}$$

where N_u and N_d are the numbers of up and down quarks, respectively.

This framework allows us to classify hadrons into isospin multiplets, where the values of I_3 vary from I to $-I$ in steps of 1:

$$I_3 = I, I-1, \ldots, -I. \tag{12.6}$$

Thus, all observed multiplets contain precisely $2I + 1$ members.

12.1.2 Analogy with Spin Quantum Numbers

The isospin quantum numbers I and I_3 are analogous to the spin quantum numbers S and S_3 used in describing the intrinsic angular momentum of particles. Just as spin quantum numbers define the possible orientations of a particle's spin, isospin quantum numbers describe the possible "orientations" of a particle's isospin within a multiplet.

For a particle with spin S, the possible values of the spin projection S_3 are given by:

$$S_3 = S, S-1, \ldots, -S. \tag{12.7}$$

Similarly, for a particle with isospin I, the possible values of I_3 were mentioned in (12.6).

The addition of isospins follows the same rules as the addition of spins in quantum mechanics. For example, if we combine two particles with isospins I^a and I^b, the total isospin I of the system can take values ranging from $|I^a - I^b|$ to $I^a + I^b$ in integer steps:

$$I = I^a + I^b, I^a + I^b - 1, \ldots, |I^a - I^b|, \tag{12.8}$$

and the third component of isospin for the combined system is simply the sum of the third components of the individual isospins:

$$I_3 = I_3^a + I_3^b. \tag{12.9}$$

This analogy between isospin and spin is not just a mathematical convenience; it reflects the underlying symmetry principles in quantum mechanics[6]

12.1.3 Example: The Sigma Baryons

The sigma baryons (Σ) provide a clear example of isospin symmetry in action. Consider the following reactions:

$$K^- + p \to \pi^+ + \Sigma^-, \quad \Sigma^+ \to \pi^+ + n, \quad \pi^0 + p, \tag{12.10}$$

where the Σ^+ baryon (uus) is part of an isospin triplet with $\Sigma^0(uds)$ and $\Sigma^-(dds)$. The third component of isospin, I_3, takes values of 1, 0, and -1 for Σ^+, Σ^0, and Σ^-, respectively.

12.2 The Least Massive Hadrons

The least massive hadrons are composed of the u, d, and s quarks, which have zero orbital angular momentum. These states include the least massive mesons and baryons, whose quantum numbers match closely with the least massive experimentally observed hadrons. Since the particles we discuss have zero charm, bottom, and top quark content, the hypercharge (Y) simplifies to:

$$Y = B + S, \tag{12.11}$$

12.2.1 The Less Massive Mesons

The least massive mesons observed experimentally are divided into two families based on their spin-parity J^P. These are the pseudoscalar meson nonet with $J^P = 0^-$ and the vector meson nonet with $J^P = 1^-$. Each family consists of nine mesons, as summarized in the weight diagrams in Figures 12.1[7].

[6] In physics, symmetries like isospin and spin describe how certain properties of particles remain unchanged under specific transformations. These symmetries help us predict the behavior of particles in different situations.

[7] In the weight diagrams, each meson is represented by a dot, with its position corresponding to its quantum numbers (Y, I_3). If two or more dots coincide, they are displaced slightly for clarity.

For example, the pseudoscalar nonet includes familiar mesons such as the π and K mesons:

$$\pi^0, \pi^+, \pi^-, \quad K^+, K^0, K^-, \overline{K^0}, \tag{12.12}$$

where each of these mesons has a spin-parity $J^P = 0^-$. This is characteristic of the pseudoscalar mesons.

The vector meson nonet, on the other hand, includes resonances like the ρ, ω, and ϕ mesons:

$$\rho^0, \rho^+, \rho^-, \quad \omega, \quad \phi, \tag{12.13}$$

where each of these mesons has a spin-parity $J^P = 1^-$. These are more massive than their pseudoscalar counterparts, and the K^* mesons, such as K^{*+} and K^{*0}, are examples from this nonet[8].

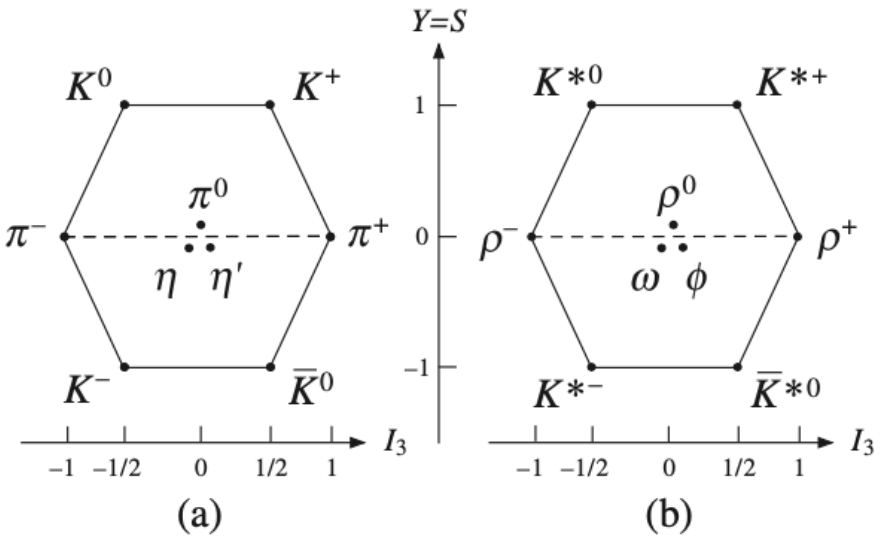

Figure 12.1: Weight diagrams for (a) the 0^- meson nonet and (b) the 1^- meson nonet.

12.2.2 Parity of Mesons

The parity of a meson depends on the orbital angular momentum L of its quark and antiquark constituents. For the least massive mesons, where $L = 0$, the parity P_M is given by:

$$P_M = P_a P_{\bar{b}} (-1)^L = (-1)^{L+1} = -1, \tag{12.14}$$

where P_a and $P_{\bar{b}}$ are the intrinsic parities of the quark and antiquark, respectively[9].

[8] The notation K^* refers to a vector meson, which is an excited state of the kaon with a spin-parity of $J^P = 1^-$. These states are more massive and can decay into their ground state counterparts.

[9] The parity of a meson is an important quantum number, reflecting the symmetry properties of its wavefunction under spatial inversion. For the least massive mesons, this parity is always -1, as derived here.

12.2.3 Quark Content and Quantum States

The quark content of these mesons is straightforward, consisting of combinations of the least massive quarks (u, d, and s) and their antiquarks. Table 12.1 provides the quantum states for the least massive $L = 0$ meson nonets. For instance to understand the properties of the K^+ meson, which has a quark content of $u\bar{s}$, we calculate its hypercharge (Y), isospin third component (I_3), and spin-parity (J^P):

The hypercharge is calculated using the formula:

$$Y = B + S, \tag{12.15}$$

where B is the baryon number, and S is the strangeness. For K^+:

- Baryon number $B = 0$ (since K^+ is a meson).
- Strangeness $S = +1$ (the strange quark contributes -1 and the anti-strange quark $\bar{s}$ contributes $+1$).

Therefore, the hypercharge Y is:

$$Y = 0 + 1 = 1. \tag{12.16}$$

The isospin third component I_3 is given by:

$$I_3 = \frac{1}{2}(N_u - N_d), \tag{12.17}$$

where N_u and N_d are the numbers of up and down quarks, respectively. For K^+ ($u\bar{s}$):

- $N_u = 1$ (one up quark)
- $N_d = 0$ (no down quarks)

Therefore, I_3 is:

$$I_3 = \frac{1}{2}(1 - 0) = \frac{1}{2}. \tag{12.18}$$

The spin-parity of K^+ is determined by its quark content and orbital angular momentum L:

- For K^+, $L = 0$ (as it is a ground state meson)
- The intrinsic parity of the quark (u) is $+1$ and for the antiquark ($\bar{s}$) it is -1

Therefore, the parity P_M is:

$$P_M = P_a P_b (-1)^L = (+1)(-1)(-1)^0 = -1. \tag{12.19}$$

Since K^+ is part of the pseudoscalar meson nonet, its total spin J is 0. Thus, the spin-parity J^P is:

$$J^P = 0^-. \tag{12.20}$$

Quark Content	0^- state	1^- state	I_3	I	$Y = S$
$u\bar{s}$	K^+ (494)	K^{*+} (892)	$1/2$	$1/2$	1
$d\bar{s}$	K^0 (498)	K^{*0} (896)	$-1/2$	$1/2$	1
$\frac{1}{\sqrt{2}}(u\bar{u} - d\bar{d})$	π^0 (140)	ρ^0 (768)*	0	1	0
$u\bar{d}$	π^+ (140)	ρ^+ (768)*	1	1	0
$d\bar{u}$	π^- (140)	ρ^- (768)*	-1	1	0
$s\bar{d}$	$\overline{K^0}$ (498)	K^{*0} (896)	$-1/2$	$1/2$	-1
$s\bar{u}$	K^- (494)	K^{*-} (892)	$1/2$	$1/2$	-1
See text	η (549)	ω (782)	0	0	0
See text	η' (958)	ϕ (1019)	0	0	0

Table 12.1: The states of the least massive $L = 0$ meson nonets.

Different members of the same isospin multiplet, such as the pions or kaons in Figure 12.1, align along horizontal lines in the weight diagrams. The consistency of internal quantum numbers across both nonets demonstrates the symmetry expected in mesons made of less massive quarks and antiquarks.

12.3 The Less Massive Baryons

The experimentally observed baryon supermultiplets include an octet of $J^P = \frac{1}{2}^+$ particles and a decuplet of $J^P = \frac{3}{2}^+$ particles. These are illustrated in Figure 12.2. The hypercharge Y for baryons is:

$$Y = S + 1 \tag{12.21}$$

The octet consists of nucleons, $\Lambda(1116)$, and Σ particles, along with the Ξ or 'cascade' particles Ξ^0 and Ξ^-, which decay via weak interactions with lifetimes around 10^{-10} s. The decuplet features $J^P = \frac{3}{2}^+$ particles, including the $\Omega^-(1672)$, which also decays through weak interactions.

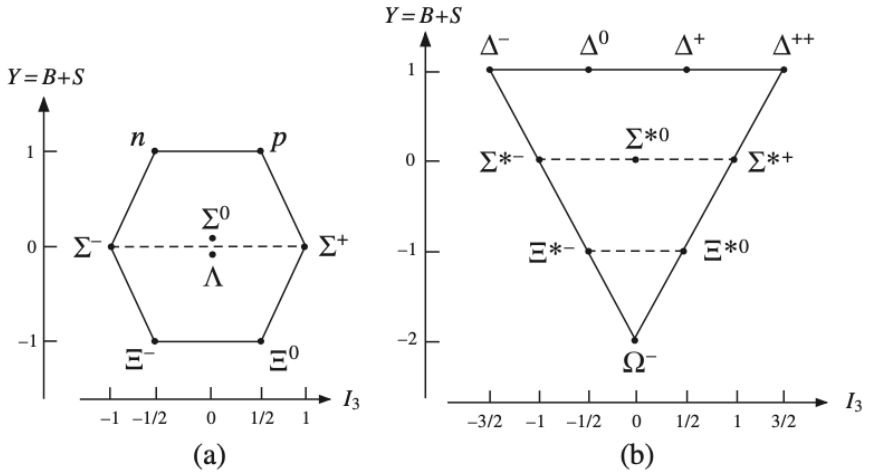

Figure 12.2: Weight diagrams for (a) the $J^P = \frac{1}{2}^+$ octet of less massive baryons and (b) the $J^P = \frac{3}{2}^+$ baryon decuplet.

The observed patterns of these states can be explained by the quark model, assuming the combined space and spin wavefunctions are *symmetric* under quark interchange. Despite quarks being spin-$\frac{1}{2}$ particles, symmetric

space-spin wavefunctions lead to the formation of octet and decuplet states.

The baryons shown in Figure 12.2 correspond to three-quark states $B = abc$ with zero orbital angular momentum, leading to a parity:

$$P = P_a P_b P_c = 1 \tag{12.22}$$

The baryon spin is the sum of the quark spins. Given the symmetric space-spin wavefunctions, the spin wavefunction must also be symmetric under the exchange of like quarks. For combinations like:

$$uud, \quad uus, \quad ddu, \quad dds, \quad ssu, \quad ssd \tag{12.23}$$

the quark pairs aa must have spin-1, leading to possible baryon spins:

$$J = S = \frac{1}{2}, \quad \frac{3}{2} \tag{12.24}$$

For symmetric combinations such as:

$$uuu, \quad ddd, \quad sss \tag{12.25}$$

all quark spins are parallel, resulting in:

$$J = S = \frac{3}{2} \tag{12.26}$$

Finally, for combinations where all quarks are different:

$$uds \tag{12.27}$$

we have two spin-$\frac{1}{2}$ baryons and one spin-$\frac{3}{2}$ baryon:

$$J = S = \frac{1}{2}, \quad \frac{1}{2}, \quad \frac{3}{2} \tag{12.28}$$

All the above states have positive parity, and by counting the various spin states in Equations (12.24), (12.26), and (12.28) we find that there are eight with $J^P = \frac{1}{2}^+$ and ten with $J^P = \frac{3}{2}^+$, as observed experimentally. Furthermore, the Y and I_3 values of the various states, obtained by adding the values for the individual quarks given in Table 12.2, correspond exactly to those of the observed states with the assignments given in Tables 12.2 and 12.3.

Quark Composition	Observed State	I_3	I	S
uud	$p(938)$	$\frac{1}{2}$	$\frac{1}{2}$	0
udd	$n(940)$	$-\frac{1}{2}$	$\frac{1}{2}$	0
uds	$\Lambda(1116)$	0	0	-1
uus	$\Sigma^+(1189)$	1	1	-1
uds	$\Sigma^0(1193)$	0	1	-1
dds	$\Sigma^-(1197)$	-1	1	-1
uss	$\Xi^0(1315)$	$\frac{1}{2}$	$\frac{1}{2}$	-2
dss	$\Xi^-(1321)$	$-\frac{1}{2}$	$\frac{1}{2}$	-2

Table 12.2: The states of the $L = 0$, $\frac{1}{2}^+$ octet of less massive baryons.

Quark Composition	Observed State	I_3	I	S
uuu	$\Delta^{++}(1232)$	$\frac{3}{2}$	$\frac{3}{2}$	0
uud	$\Delta^+(1232)$	$\frac{1}{2}$	$\frac{3}{2}$	0
udd	$\Delta^0(1232)$	$-\frac{1}{2}$	$\frac{3}{2}$	0
ddd	$\Delta^-(1232)$	$-\frac{3}{2}$	$\frac{3}{2}$	0
uus	$\Sigma^{*+}(1383)$	1	1	-1
uds	$\Sigma^{*0}(1384)$	0	1	-1
dds	$\Sigma^{*-}(1387)$	-1	1	-1
uss	$\Xi^{*0}(1532)$	$\frac{1}{2}$	$\frac{1}{2}$	-2
dss	$\Xi^{*-}(1535)$	$-\frac{1}{2}$	$\frac{1}{2}$	-2
sss	$\Omega^-(1672)$	0	0	-3

Table 12.3: The states of the $L = 0$, $\frac{3}{2}^+$ decuplet of less massive baryons.

12.4 Charmonium

The charmonium system is most effectively studied by forming states such as $V^0 = J/\psi(3097)$, $\psi(3686), \ldots$, which share the same J^{PC} values as the photon, 1^{--}[10]. The primary formation mechanism is shown in Figure 12.3. An electron-positron pair annihilates to form a virtual photon, which then converts to V^0, decaying mainly into hadrons. This occurs when the center-of-mass energy equals the mass of V^0, leading to a peak in the total cross-section for electron-positron annihilation into hadrons.

The cross-section ratio R is typically plotted as:

$$R \equiv \frac{\sigma(e^+e^- \to \text{hadrons})}{\sigma(e^+e^- \to \mu^+\mu^-)}\,, \tag{12.29}$$

Where the cross-section for muon pair production is:

$$\sigma(e^+e^- \to \mu^+\mu^-) = \frac{4\pi\alpha^2}{3E_{CM}^2}\,, \tag{12.30}$$

This ratio R varies smoothly with the center-of-mass energy E_{CM}.

As depicted in Figure 12.4, there are two sharp peaks corresponding to the masses of $J/\psi(3097)$ and $\psi(3686)$, with broader peaks at higher energies above 3730 MeV. This higher energy is referred to as the *charm threshold*, which is approximately twice the mass of the lightest charmed particles, the D mesons. Above this threshold, charmonium states decay quickly into pairs of charmed particles. Below this threshold, the states decay more

[10]The photon has the quantum numbers $J^{PC} = 1^{--}$, which means it has spin-1, parity-odd, and charge conjugation symmetry.

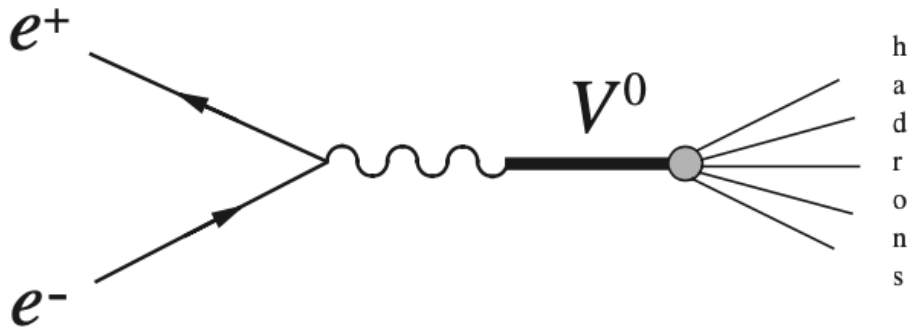

Figure 12.3: Mechanism for the formation of mesons V^0 with quantum numbers $J^{PC} = 1^{--}$ in electron-positron annihilation, followed by decay to hardons.

slowly into non-charmed hadrons[11].

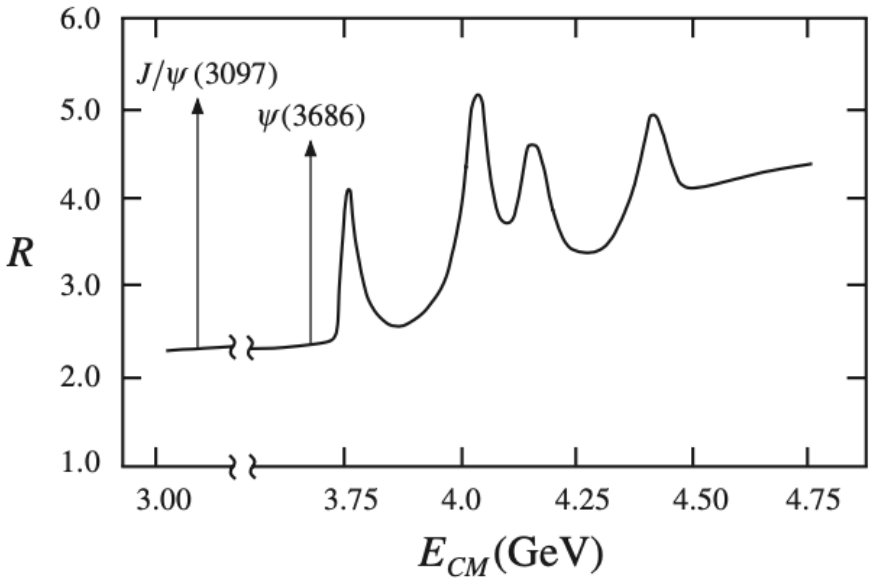

Figure 12.4: The cross-section ratio R as a function of center-of-mass energy E_{CM}, showing the narrow peaks corresponding to $J/\psi(3097)$ and $\psi(3686)$.

12.4.1 Above and Below the Charm Threshold

The decay mechanisms differ above and below the charm threshold. Above the threshold, charmonium states decay primarily into pairs of charmed quark-antiquark pairs, as shown in Figure 12.5a. Below the threshold, they decay into non-charmed mesons, as depicted in Figure 12.5b.

The $J/\psi(3097)$ and $\psi(3686)$ are the best-known charmonium states, with the same $J^{PC} = 1^{--}$ quantum numbers as the photon. Other states can be found by studying the radiative decays of these two, as shown in the following equations:

[11] States below the charm threshold are easier to identify experimentally due to their narrow decay widths. These states typically decay via mechanisms involving lower-energy hadrons.

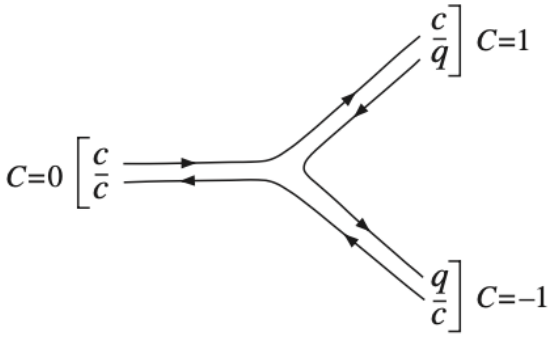

(a) Decay of a charmonium state to a pair of charmed mesons.

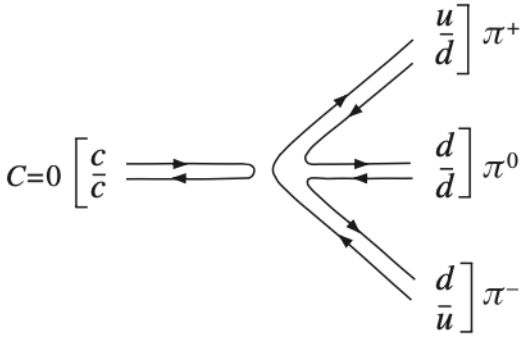

(b) An example of a decay to non-charmed mesons.

Figure 12.5: Quark diagrams for (a) the decay of a charmonium state to a pair of charmed mesons and (b) an example of a decay to non-charmed mesons.

$$\psi(3686) \to \chi_{ci} + \gamma \quad (i = 0, 1, 2) \quad \text{(Branching Ratio: } \sim 28\%), \tag{12.31}$$

$$J/\psi(3097) \to \eta_c(2980) + \gamma \quad \text{(Branching Ratio: } \sim 1\%), \tag{12.32}$$

Where χ_{ci} represents new charmonium states known as chi-states, which decay mostly to hadrons.

12.4.2 Charmonium Spectrum and Radiative Transitions

All eight predicted states of charmonium with principal quantum number $n \leq 2$ have been identified, as shown in the spectrum in Figure 12.6.

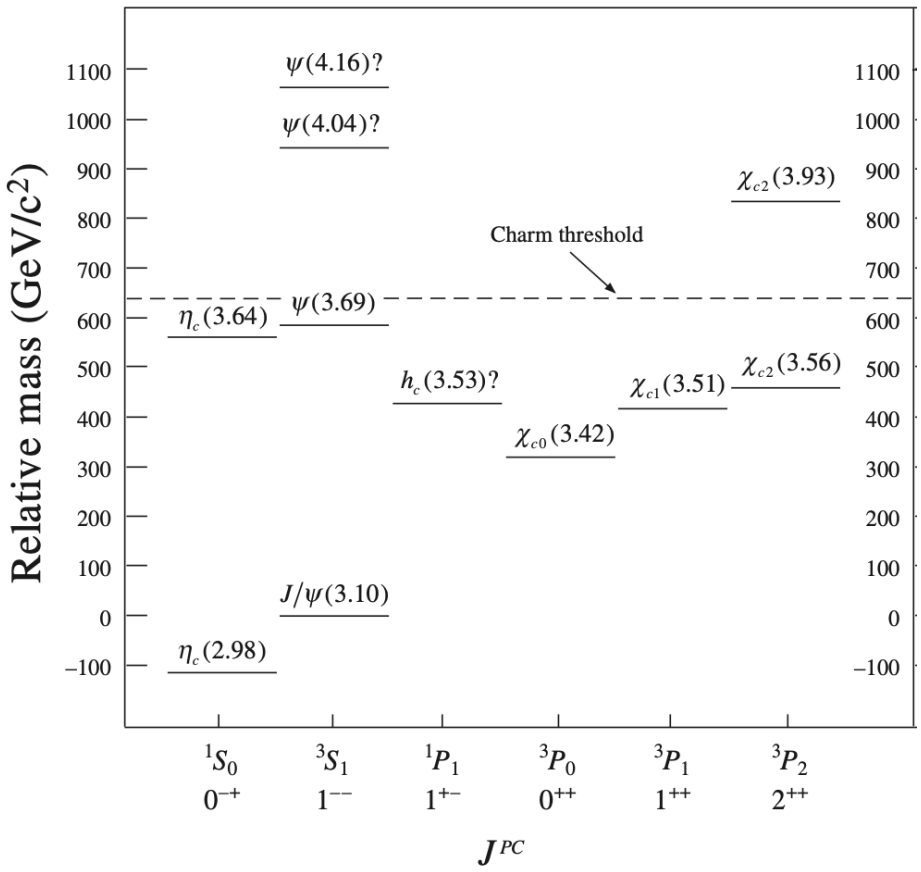

Figure 12.6: Charmonium spectrum, showing radiative transitions and the charm threshold.

QCD, Jets and Gluons

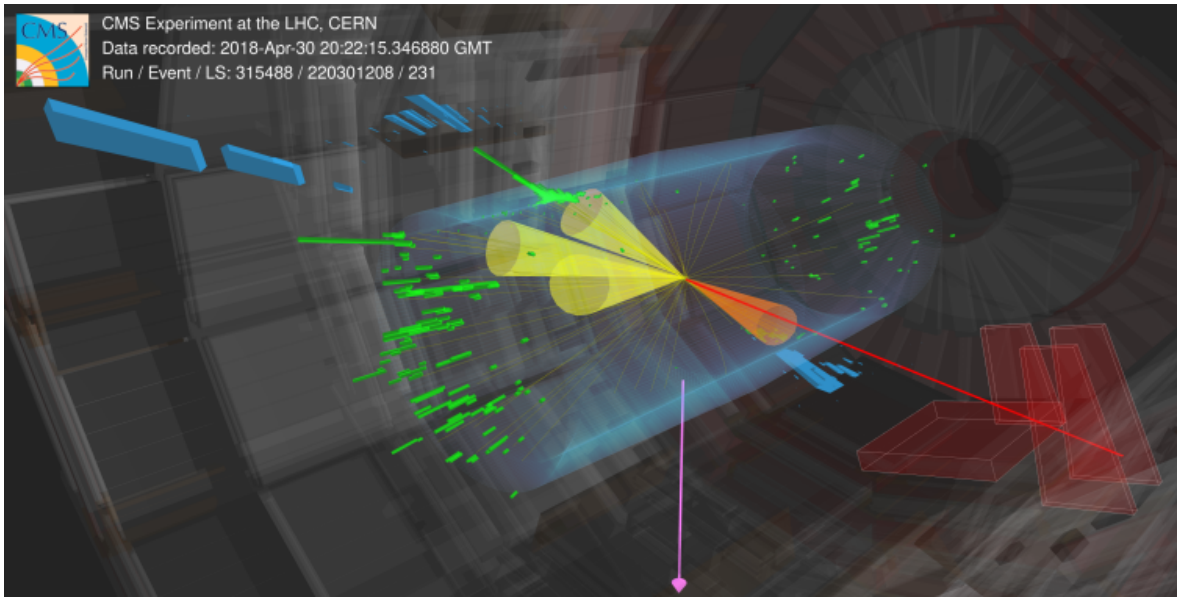

Figure 13.1: The CMS detector recorded the event, showing a top quark pair decay. One top quark decays into three quarks (yellow jets), the other into a b quark, a muon (red line), and an undetected neutrino. Jets are orange and yellow cones, with signals in the calorimeters displayed by green (electromagnetic) and blue (hadron) bars. Muon chamber signals are indicated by red boxes and missing momentum is represented by pink arrow.

This chapter explores the fundamental aspects of Quantum Chromodynamics (QCD), jets, and gluons. The figure above illustrates a top quark pair decay, where one top quark decays into three quarks (forming jets, shown as orange and yellow cones), and the other into a b quark, a muon (red line), and an undetected neutrino. Jets, which are streams of particles resulting from quark and gluon interactions, provide insights into the strong force binding these particles together.

13.1 Quantum Chromodynamics (QCD)

Quantum Chromodynamics (QCD) is a gauge theory[1] that underpins our understanding of strong interactions within the Standard Model of particle physics. Gauge theories involve interactions between particles governed by a symmetry known as gauge invariance[2]. The force-mediating particles in QCD are the gluons, which, unlike photons in Quantum Electrodynamics (QED), carry the color charge[3] and thus participate in more complex interactions. These self-interactions among gluons lead to unique phenomena in QCD, such as color confinement[4], where quarks and gluons cannot exist independently, and asymptotic freedom[5], where the force between quarks diminishes as they approach each other.

13.1.1 QED vs. QCD

Although both QED and QCD are gauge theories involving massless spin-1 bosons—photons in QED and gluons in QCD—there are significant differences. In QED, the photon interacts only with electric charge. In contrast, in QCD, the gluon couples to the color charge and can interact with other gluons, resulting in a richer structure of interactions.

Figure 13.2 visually compares the interactions in QED and QCD, highlighting the self-interactions of gluons that are unique to QCD.

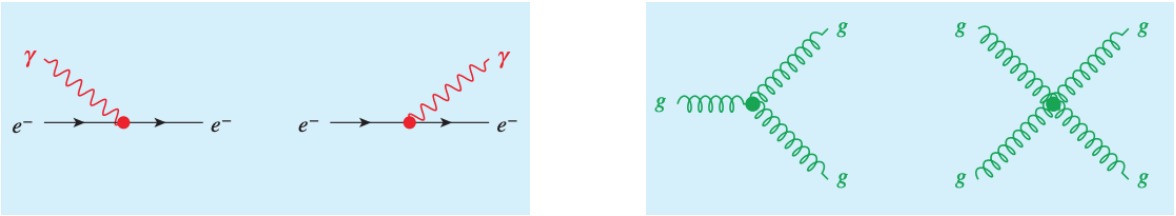

(a) Photon-Electron Interaction

(b) Gluon-Gluon Interaction

Figure 13.2: Comparative diagrams illustrating (a) photon-electron interactions in QED and (b) gluon-gluon interactions in QCD, emphasizing the unique self-interactions of gluons.

13.1.2 Color Charge and Confinement

In QCD, quarks and gluons are characterized by color charge, which exists in three varieties: red, green, and blue[6]. This property results in color confinement, a phenomenon where quarks and gluons form color-neutral combinations, leading to the observation of only colorless particles, such as protons and neutrons. The concept of color confinement is a tool for explaining why we do not observe free quarks or gluons in nature; instead, they are always confined within hadrons, such as protons and neutrons.

[1] A type of field theory where a symmetry principle governs interactions.
[2] A principle ensuring consistency of physical laws under local transformations.
[3] A property that allows quarks and gluons to interact strongly.
[4] Quarks and gluons are bound together and cannot be isolated.
[5] The strong force weakens as quarks get closer.
[6] Labels for the charge type in the strong interaction, not actual colors.

13.1.3 Asymptotic Freedom

Asymptotic freedom is another fundamental property of QCD, where the strength of the strong interaction decreases as quarks come closer together, allowing them to behave almost freely at short distances. Conversely, as quarks separate, the interaction strength increases, effectively preventing their isolation—an inverse behavior to what is observed in QED.

13.1.4 Gluon Interactions and Gauge Invariance

In QCD, gluons carry color charges and interact with one another, leading to a complex array of gluon-gluon interactions. These interactions are governed by gauge invariance, which ensures that the laws of physics remain consistent under local transformations of the color charge. Gauge invariance necessitates that gluons are massless and that the strong force between quarks is mediated through gluon exchange. This principle also permits gluon self-interactions, a distinctive feature of QCD that differentiates it from QED.

Figure 13.3 illustrates the exchange of color charge between quarks and the self-interactions among gluons, demonstrating the fundamental processes that govern QCD.

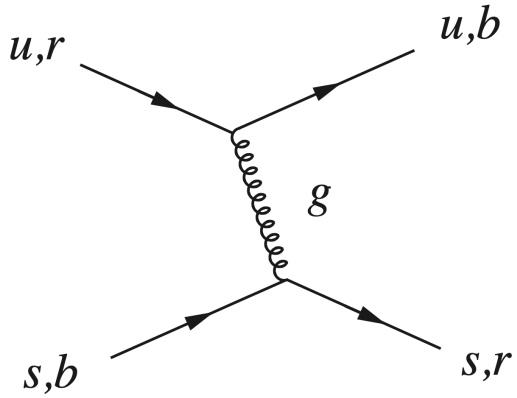

Figure 13.3: Illustrations of quark-quark and gluon-gluon scattering in QCD, demonstrating the exchange of color charge.

13.1.5 Jets and Their Formation

Jets are collimated streams of particles that result from the hadronization of quarks and gluons produced in high-energy collisions. Due to the nature of the strong force, quarks and gluons cannot exist as free particles; instead, they fragment[7] into a cascade of stable particles, which then form jets.

An intuitive analogy for understanding jets can be drawn using an ice cream cone. Imagine an ice cream cone with three different flavored scoops. Each scoop represents a different type of quark flavor—such as up, down, and strange quarks—that contribute to the formation of the jet. The cone itself is analogous to the jet structure, where all flavors are bound together by a strong force, just as the ice cream scoops are held together by the

[7] Fragmentation refers to the process where quarks and gluons, unable to exist freely due to the strong force, break apart into hadrons, which are the observed particles in jets.

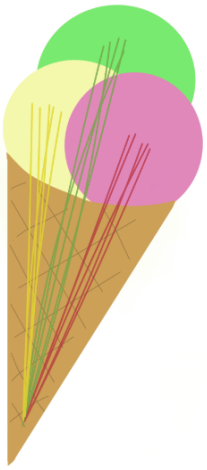

Figure 13.4: An illustration of a jet cone with top flavor, represented as an ice cream cone with three flavors.

cone. The top quark, due to its large mass, decays in a way that can result in a jet resembling an ice cream cone, with multiple flavors present within a single jet.

13.2 The Strong Coupling Constant

The strong interaction, responsible for binding quarks together within hadrons, is characterized by a force that operates at very short distances, typically on the order of 1 fm (femtometer). This interaction becomes weaker as quarks come closer together, a property known as *asymptotic freedom*. The magnitude of this interaction is quantified by the *strong coupling constant* α_s. The strong coupling constant α_s depends on the energy scale μ at which it is measured. As the energy increases, the value of α_s decreases, indicating that the interaction weakens at shorter distances. This relationship is described by the *running of the coupling constant* and is a fundamental prediction of Quantum Chromodynamics (QCD).

$$\alpha_s(\mu) = \alpha_s(\mu_0) \left[1 + \frac{33 - 2N_f}{6\pi} \alpha_s(\mu_0) \ln\left(\frac{\mu}{\mu_0}\right)\right]^{-1} \tag{13.1}$$

where:

- $\alpha_s(\mu)$ is the strong coupling constant at the energy scale μ,
- N_f is the number of quark flavors,
- μ is the energy scale,
- μ_0 is a reference scale, typically taken to be the mass of the Z boson (M_Z).

The running coupling constant $\alpha_s(\mu)$ provides an insight into the behavior of quarks within hadrons and the interactions that govern their dynamics. As depicted in Figure 13.5, as μ increases (corresponding to smaller distances between quarks), α_s decreases, confirming the weakening of the strong force at short distances or in other words, asymptotic freedom.

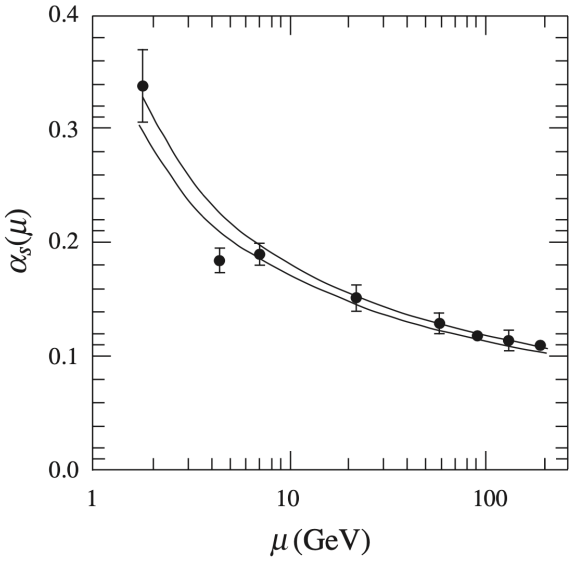

Figure 13.5: Values of the running coupling constant α_s as a function of the energy scale μ. The curve illustrates how α_s decreases with increasing μ, consistent with the property of asymptotic freedom.

13.3 Electron-Positron Annihilation

In the process of electron-positron annihilation, an electron (e^-) and a positron (e^+) collide and annihilate, typically resulting in the production of hadrons or muons. This interaction occurs at high energies in a particle collider, making it a fundamental process in studying the strong force and the behavior of quarks and gluons.

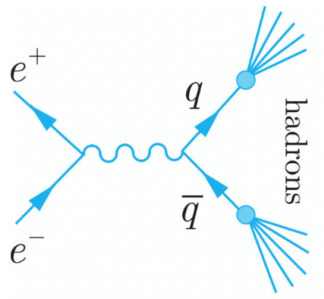

Figure 13.6: Diagram illustrating the basic mechanism of two-jet production in electron-positron annihilation.

13.3.1 Two-Jet Events

In the energy range of 15–40 GeV, electron-positron annihilation into hadrons is typically dominated by the production of quark-antiquark pairs ($q\bar{q}$). These quark pairs hadronize into jets, which are collimated streams of particles moving in similar directions. The reaction can be written as:

$$e^+ + e^- \to q + \bar{q} \tag{13.2}$$

- e^+ and e^-: Positron and electron respectively, which annihilate.

- q and $\bar{q}$: Quark and antiquark pair produced from the annihilation.

The two jets formed are usually emitted back-to-back due to the conservation of momentum[8]. The angular distribution of these jets can be analyzed to reveal the properties of the initial quark-antiquark pairs. In practice, this process is observed as two jets of hadrons, and the direction of each jet reflects the original direction of the quark and antiquark.

13.3.2 Validation Through Angular Distribution

The interpretation of two-jet events is confirmed by comparing their angular distribution with the angular distribution of muons in the reaction:

$$e^+ + e^- \to \mu^+ + \mu^- \tag{13.3}$$

- μ^+ and μ^-: Muon and antimuon pair produced in the annihilation.

This process is theoretically identical to the quark-antiquark production in two-jet events, making it a useful reference for validating the observed angular distributions of jets[9]. If the angular distribution of jets is consistent with the distribution from $\mu^+\mu^-$ pairs, it supports the conclusion that the jets originated from quark-antiquark pairs.

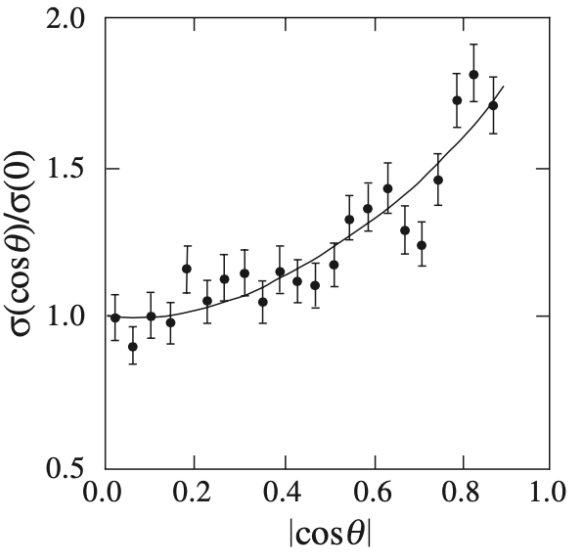

Figure 13.7: Comparison of angular distributions in two-jet events and muon pair production.

13.3.3 Differential Cross-Section

At high beam energies $E \gg m_\mu$, the differential cross-section for muon pair production is:

[8]Momentum is a measure of the motion of a particle, and it is conserved in isolated systems. This means that the total momentum before and after the annihilation remains the same.

[9]The angular distribution refers to the pattern of angles at which particles are emitted after a collision. In a two-jet event, jets are typically emitted in opposite directions.

$$\frac{d\sigma}{d\cos\theta}(e^+e^- \to \mu^+\mu^-) = \frac{\pi\alpha^2}{8E^2}(1+\cos^2\theta) \tag{13.4}$$

- θ: Production angle of either muon with respect to the initial electron direction.
- α: Fine structure constant, a fundamental constant characterizing the strength of electromagnetic interactions.
- E: Center-of-mass energy, the total energy available in the system's center of mass.

For quark-antiquark pairs of a given flavor a, the cross-section is similarly obtained by replacing the muon charge e_μ with the quark charge e_a, and multiplying by three to account for the three possible color states (red, green, blue):

$$\frac{d\sigma}{d\cos\theta} = \frac{3\pi e_a^2\alpha^2}{8E^2}(1+\cos^2\theta) \tag{13.5}$$

13.3.4 Three-Jet Events and Gluon Radiation

In addition to two-jet events, three-jet events can also occur if a high-momentum gluon is emitted before hadronization. The production of a three-jet event can be represented as:

$$e^+ + e^- \to q + \bar{q} + g \tag{13.6}$$

- g: Gluon emitted by the quark or antiquark before hadronization.

Such three-jet events provide strong evidence for the existence of gluons. These events are more complex to analyze because the gluon emission is not directly observable, but the resulting jets can be studied to infer the presence of the gluon. The angular distribution of the jets in three-jet events is crucial for determining the strong coupling constant α_s, which governs the strength of the interaction.

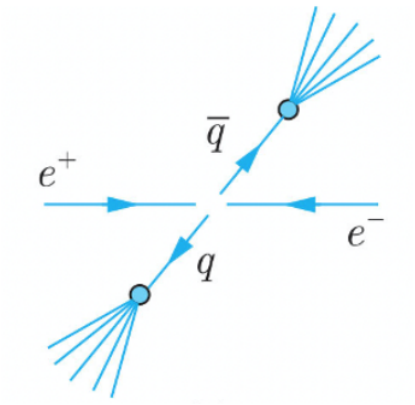

(a) Two-jet formation in electron-positron annihilation.

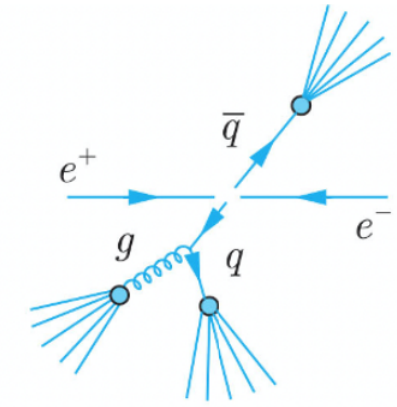

(b) Three-jet formation in electron-positron annihilation.

Figure 13.8: Schematic diagrams representing (a) two-jet and (b) three-jet formation in electron-positron annihilation in the center-of-mass frame.

13.3.5 Cross-Section Ratios

The cross-section ratio R is defined as:

$$R = \frac{\sigma(e^+e^- \to \text{hadrons})}{\sigma(e^+e^- \to \mu^+\mu^-)} \tag{13.7}$$

This ratio provides a measure of the relative likelihood of hadron production compared to muon pair production[10]. If hadron production is dominated by two-jet events, the ratio can be approximated as:

$$R_0 = N_c \left(e_u^2 + e_d^2 + e_s^2 + e_c^2 + e_b^2\right) = 11N_c/9 \tag{13.8}$$

where $N_c = 3$ is the number of color states. If three-jet events and higher-order corrections are included, the ratio is modified to:

$$R = R_0 \left(1 + \frac{\alpha_s}{\pi}\right) \tag{13.9}$$

This modification accounts for the small contributions from gluon radiation and other effects that are not captured in the simplest two-jet model.

13.3.6 Discussion

Which quarks contribute to R_0 at 2.8 GeV and 5 GeV?

Answer: At 2.8 GeV, the contributing quarks are u, d, and s, while at 5 GeV, c quarks also contribute.

Why does R_0 involve only 5 flavors of quarks?

Answer At the energies in question, only five flavors (up, down, strange, charm, and bottom) are produced. The top quark is too massive to be produced at these energies.

[10]The cross-section is a measure of the probability of a specific interaction occurring. A higher cross-section indicates a more likely interaction.

Higgs Boson

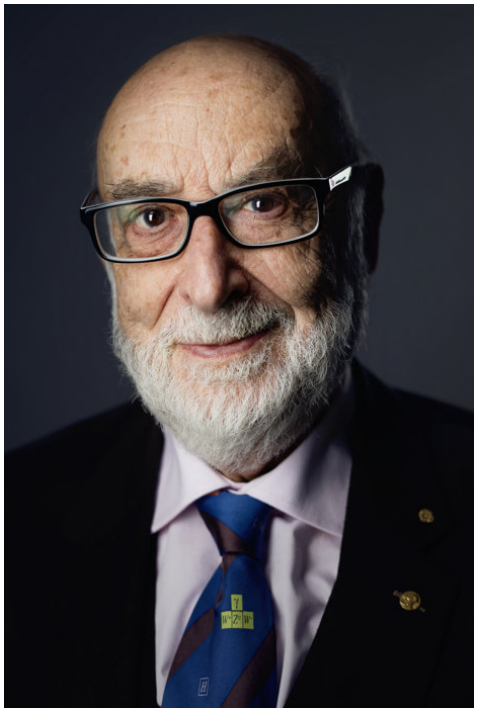

(a) François Englert

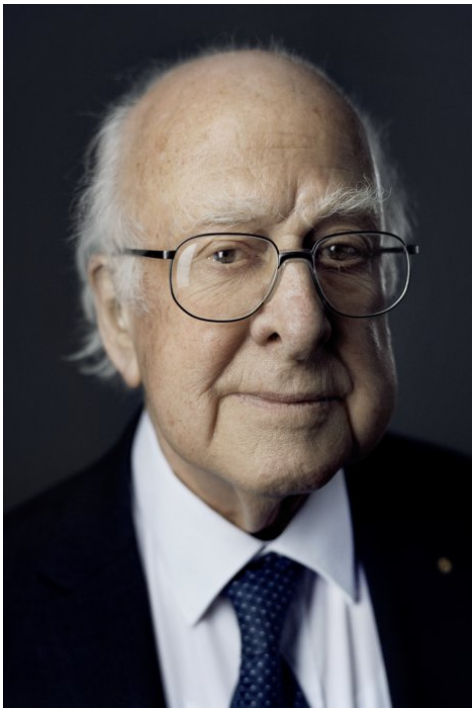

(b) Peter W. Higgs

Figure 14.1: François Englert and Peter W. Higgs, recipients of the 2013 Nobel Prize in Physics.

The Higgs boson is a neutral spin-0 particle that plays a crucial role in the Standard Model of particle physics. This particle is essential because of the principle of gauge invariance, which, within the framework of quantum field theory, demands that spin-1 gauge bosons, such as the photon and gluon, be massless. However, the weak interaction, mediated by the $W^{\pm}$ and Z^0 bosons, presents a paradox as these bosons are indeed massive.

This apparent contradiction was resolved through the concept of spontaneous symmetry breaking[1], a mechanism proposed in the 1960s. The Higgs field, a scalar field permeating all of space, interacts with the gauge bosons, enabling them to acquire mass while preserving the underlying gauge symmetry. This process, known

[1] Symmetry breaking occurs when a symmetric system becomes asymmetric under certain conditions, leading to mass acquisition for particles.

as the Higgs mechanism, elegantly reconciles the need for massive $W^{\pm}$ and Z^0 bosons within a gauge-invariant theory.

The development of this theory is credited to three pioneers: **Peter Higgs**, who independently proposed the idea, and **François Englert** and **Robert Brout**, who collaborated on it. In 1964, Peter Higgs proposed the idea of spontaneous symmetry breaking in gauge theories independently, while François Englert and Robert Brout worked together on a similar concept. This groundbreaking idea has since become a cornerstone of modern particle physics. For their contributions, Peter Higgs and François Englert were awarded the Nobel Prize in Physics in 2013. Unfortunately, Robert Brout, who passed away in 2011, was not eligible to share in the Nobel Prize, as the award cannot be given posthumously.

14.1 Higgs Field

The Higgs field is a scalar field that gives mass to gauge bosons in the Standard Model. Unlike other fields, the Higgs field has a nonzero value in the vacuum, denoted by η_0. This nonzero value breaks the gauge invariance but allows the $W^{\pm}$ and Z^0 bosons to acquire mass. As a result, the symmetry of the vacuum is broken, leading to spontaneous symmetry breaking.

The Higgs mechanism explains how gauge bosons gain mass while photons remain massless. This process is essential for the consistency of the Standard Model, ensuring that the theory matches observed particle behaviors. The Lagrangian for the Higgs field is:

$$\mathcal{L}_{\text{Higgs}} = \frac{1}{2}(\partial_\mu \phi)^2 - V(\phi), \tag{14.1}$$

where $V(\phi)$ represents the potential leading to mass generation. This process is key to the Standard Model, ensuring that only the $W^{\pm}$ and Z^0 bosons gain mass.

14.1.1 Higgs Field and Potential Energy

The Higgs field is special because it has a nonzero value even in the vacuum, unlike other fields such as the electromagnetic (EM) field, which vanishes in the vacuum state.

To visualize this, consider the potential energy $V(\eta)$ of the Higgs field, which has a minimum not at zero but at a nonzero value. This results in a ”Mexican hat” or ”champagne bottle” shape for the potential, as shown in Figure 14.2b. On the other hand, the EM field’s potential reaches its minimum at zero, as shown in Figure 14.2a.

This difference can be understood through a simple analogy: imagine a ball rolling inside a bowl (the EM field), which naturally comes to rest at the lowest point, zero. In contrast, the Higgs field is like a ball rolling inside a ring-shaped trough (the ”Mexican hat” potential), where the lowest energy state is along a circle, not at the center, which corresponds to a nonzero value.

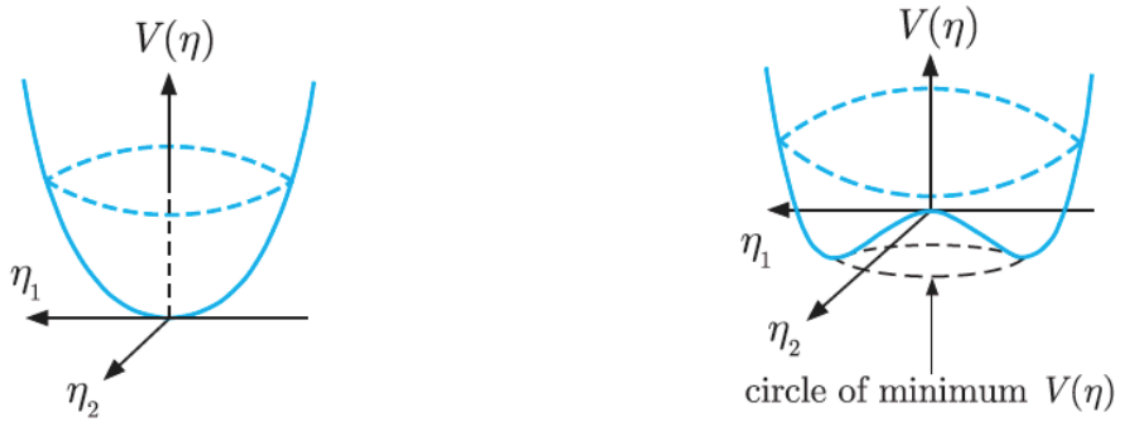

(a) EM Field Potential

(b) Higgs Field Potential

Figure 14.2: Comparison of Potential Energy between EM Field and Higgs Field. (a) The potential of the EM field reaches its minimum at zero. (b) The Higgs field has a nonzero minimum, resulting in a "Mexican hat" potential.

This configuration ensures that the Higgs field does not vanish in the vacuum, leading to mass acquisition for the gauge bosons, which is essential for the Standard Model to work correctly.

14.2 Higgs Mechanism

The Higgs mechanism is a process by which gauge bosons acquire mass through their interaction with the non-vanishing vacuum expectation value of the Higgs field. This process is fundamental to the Standard Model of particle physics, where it explains why the $W^{\pm}$ and Z^0 bosons have mass, while the photon remains massless.

The Higgs mechanism has three main consequences:

1. The $W^{\pm}$ and Z^0 bosons acquire masses, allowing for the weak force to have a short range.
2. The existence of a new electrically neutral particle, the Higgs boson (denoted as H^0), which is associated with the quanta of the Higgs field, similar to how photons are quanta of the electromagnetic field.
3. The generation of fermion masses through interactions with the Higgs field, a result of the nonzero vacuum expectation value of the Higgs field.

Initially, the universe existed in a symmetric state where the electromagnetic and weak forces were unified, and all particles were massless. As the universe cooled, it transitioned into a less symmetric state, causing the electroweak symmetry to break spontaneously. This led the Higgs field to acquire a nonzero vacuum expectation value (VEV) of 246 GeV, giving mass to the $W^{\pm}$ and Z^0 bosons. The remaining component of the Higgs field manifests as the Higgs boson. Fermion masses, such as those of electrons and quarks, arise from their interactions with the Higgs field via Yukawa couplings[2].

In Figure 14.3, the "Mexican hat" potential is depicted, where the universe is pictured as initially being at the top of the hat in a symmetric state. As the universe cools, it moves down to a lower energy state along the rim

[2] Yukawa couplings describe the interaction between the Higgs field and fermions, leading to the generation of fermion masses.

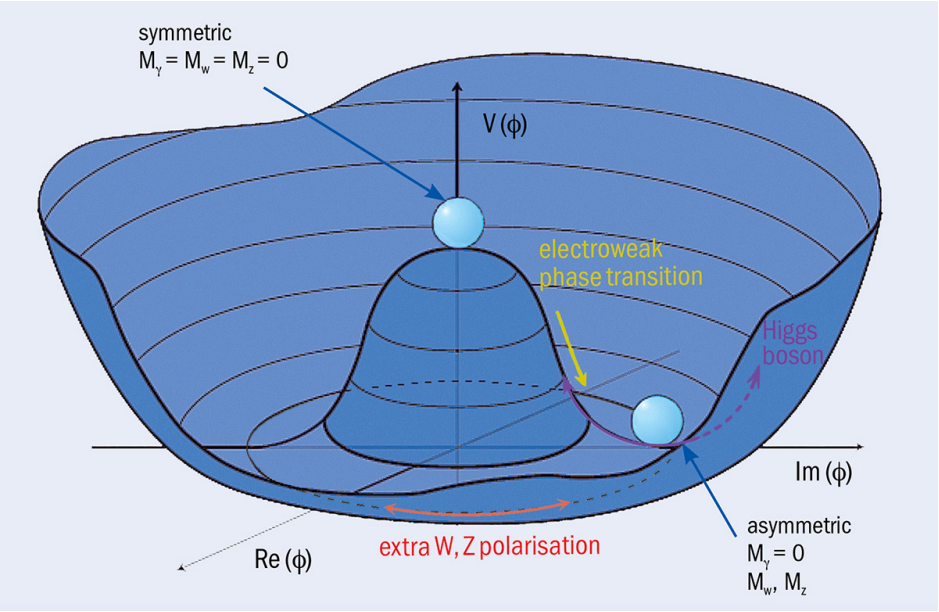

Figure 14.3: The "Mexican hat" potential represents the Higgs field. The universe transitions from a symmetric state at the top of the potential to a less symmetric state along the rim, giving rise to the masses of the $W^{\pm}$ and Z^0 bosons and the Higgs boson.

of the hat, representing the electroweak phase transition. This transition results in the acquisition of mass by the $W^{\pm}$ and Z^0 bosons due to their interaction with the Higgs field, while the Higgs boson is associated with the remaining degree of freedom in the field.

14.3 Higgs Boson Production

14.3.1 LEP and Higgs Production

The existence of the Higgs boson is one of the most critical predictions of the Standard Model. The Large Electron-Positron Collider (LEP) at CERN, with a maximum energy of 208 GeV, attempted to discover the Higgs boson. However, LEP could only explore Higgs boson masses up to around 120 GeV, which was insufficient for its discovery.

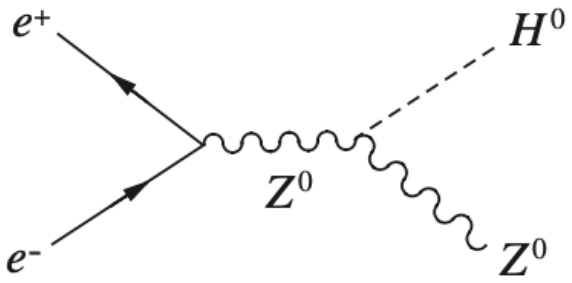

Figure 14.4: Feynman diagram for Higgs boson production at LEP. An electron and positron annihilate, producing a Z boson that decays into a Higgs boson and another Z boson.

Despite the efforts, LEP's energy was not high enough to produce the more massive Higgs bosons. This

limitation led to LEP's closure in November 2002 without observing the Higgs boson.

14.3.2 LHC and Higgs Production

The Large Hadron Collider (LHC) at CERN succeeded where LEP could not. The LHC began operations with an initial energy of 7 TeV, later increasing to 13 TeV. The dominant production mechanism for the Higgs boson at the LHC is gluon fusion, where two gluons interact to produce a Higgs boson.

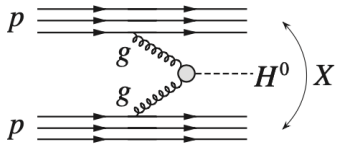

(a) Gluon fusion.

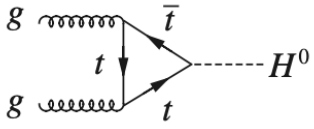

(b) Top quark loop.

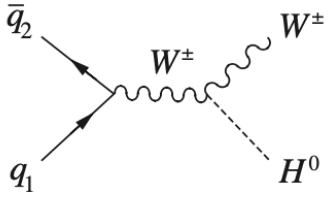

(c) W boson fusion.

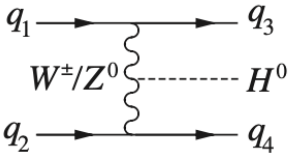

(d) Z boson fusion.

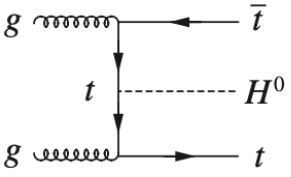

(e) Associated production with top quark pairs.

Figure 14.5: Higgs boson production mechanisms at the LHC. These include (a) gluon fusion, (b) top quark loop, (c) W boson fusion, (d) Z boson fusion, and (e) associated production with top quark pairs.

In 2012, the LHC's increased energy and advanced detection capabilities led to the discovery of the Higgs boson.

Figure14.5 illustrates the primary mechanisms for Higgs boson production at the LHC, including gluon fusion and associated production with top quarks. The LHC's success lies in its ability to probe the higher energy scales required to produce and detect the Higgs boson.

14.4 Higgs Boson Decays at the LHC

The discovery of the Higgs boson at the LHC was primarily based on observing its decay into specific channels. The branching ratios of these decay channels, as shown in Figure 14.6, play a crucial role in determining which decay modes were observed first.

14.4.1 Detected Decay Channels

The first successful detection of the Higgs boson came through the following decay channels:

- **Higgs Decay to Two Photons:**

$$H^0 \to \gamma\gamma \tag{14.2}$$

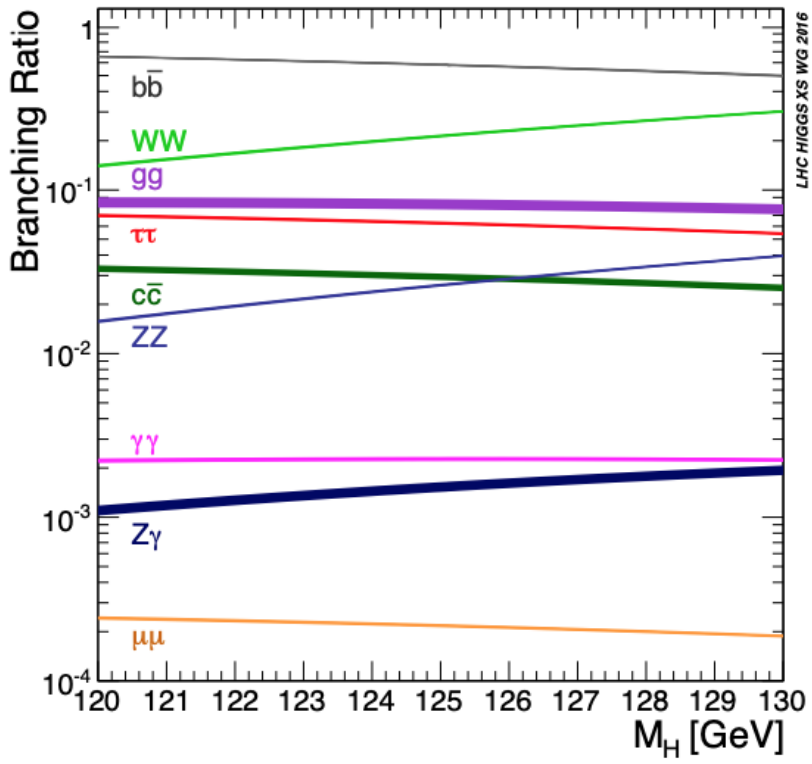

Figure 14.6: Branching ratios of various Higgs boson decay channels as a function of the Higgs boson mass. The first observed decays were through channels with the most significant branching ratios at a mass of around 125 GeV.

This channel, despite having a relatively small branching ratio, was detected early due to the clean experimental signature of photons in the detectors and lower background noise.

- **Higgs Decay to Four Leptons (via Two Z Bosons):**

$$H^0 \to ZZ \to 4\ell \tag{14.3}$$

This channel also provided a clear and distinct signature with low background noise, making it one of the first to be observed. The decay into four leptons (electrons or muons) offers a precise way to reconstruct the Higgs boson mass.

14.4.2 Undetected or Later Detected Channels

Several other decay channels were either undetected or only observed later, primarily due to the following reasons:

- **Higgs Decay to Bottom Quarks:**

$$H^0 \to b\bar{b} \tag{14.4}$$

Although this channel has the highest branching ratio, it was not initially observed due to the high background from QCD processes that produce many bottom quark pairs, making it challenging to isolate

the Higgs signal.

- **Higgs Decay to W Bosons:**

$$H^0 \to W^+W^- \tag{14.5}$$

The decay into W bosons has a substantial branching ratio, but the final states can be challenging to identify due to the presence of neutrinos in the final state, which escape detection, making it harder to fully reconstruct the event.

- **Higgs Decay to Tau Leptons:**

$$H^0 \to \tau^+\tau^- \tag{14.6}$$

The detection of this channel is complicated by the fact that taus decay into neutrinos and other particles, which leads to missing energy in the detector, complicating the event reconstruction.

The initial discovery channels were those with clean signatures and low background, allowing for a clear identification of the Higgs boson even with the relatively small amount of data collected in the early stages of the LHC. As data collection continued and techniques improved, other decay channels were observed, confirming the properties of the Higgs boson and providing a more comprehensive understanding of its behavior.

14.5 Higgs Boson Mass Determination

The mass of the Higgs boson was one of the critical unknowns in the Standard Model before its discovery. The graph in Figure 14.7 shows the four-lepton mass distribution for the decay channel $H^0 \to ZZ \to 4\ell$, which played a role in pinpointing the mass of the Higgs boson.

In the graph, the excess of events around 125 GeV corresponds to the mass of the Higgs boson. The red line in the histogram represents the expected signal for a Higgs boson with a mass of 125 GeV, and the blue shading indicates the background from other processes. The clear peak around 125 GeV in the four-lepton mass distribution provides compelling evidence for the existence of the Higgs boson with this mass.

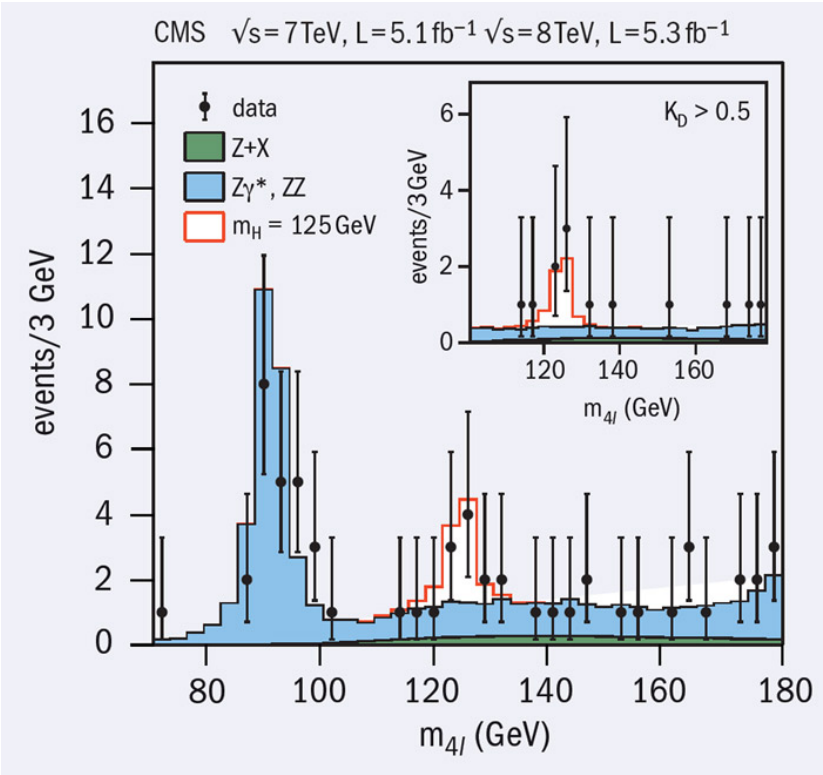

Figure 14.7: Four-lepton mass for the $H \to ZZ \to 4\ell$ decay mode. The insert highlights the events passing a kinematic discriminant that selects Higgs-like decay topologies.

Discrete Symmetries

Charge conjugation (C) and parity (P) are exact symmetries of strong and electromagnetic interactions. However, in the context of weak interactions, these symmetries are not conserved, which leads to significant consequences.

Two key interconnected themes emerge when discussing C and P in weak interactions:

- **Spin Dependence:** The violation of these symmetries in weak interactions is linked to the spin dependence of these interactions, which is a remarkable feature.
- **CP Invariance:** While individual C and P symmetries are violated, there exists a weaker combined symmetry called CP invariance. CP invariance seems to be exactly conserved in the weak interactions of leptons.

However, experimental evidence suggests deviations from this invariance when extending CP invariance to the weak interactions of hadrons. These deviations have significant implications.

15.1 Overview of CP and CPT Invariance

- **CP Invariance in Leptons:** CP symmetry appears to be conserved in leptonic weak interactions, meaning that when both C and P transformations are applied, the overall symmetry holds.
- **CP Violation in Hadrons:** There is experimental evidence for CP violation in hadronic weak interactions, which means that this combined symmetry does not always hold, leading to deviations.
- **CPT Invariance:** CPT symmetry, which combines charge conjugation (C), parity transformation (P), and time reversal (T), is believed to be conserved in all interactions. This symmetry is considered more fundamental and universal.

These concepts are explored further in dedicated sections, where the nature and implications of CP and CPT invariance are discussed in detail, particularly in the context of the Standard Model and ongoing experiments.

15.2 P-Violation in Weak Interactions

Parity (P) was initially believed to be a universal symmetry, conserved across all types of interactions, similar to angular momentum conservation. However, this assumption was challenged by experiments on weak interactions, particularly those involving the decay of polarized Cobalt-60 nuclei.

15.2.1 Cobalt-60 Decay and Parity Violation

In an experiment conducted by Wu[1] and collaborators in 1957, Cobalt-60 nuclei were placed inside a solenoid and cooled to 0.01 K. At this temperature, the nuclear spins align parallel to the magnetic field direction. The nuclei then undergo beta decay, transitioning to an excited state of Nickel-60:

$$^{60}\text{Co} \rightarrow ^{60}\text{Ni}^{*} + e^{-} + \overline{\nu}_e \tag{15.1}$$

The key observation from this experiment was a 'forward-backward decay asymmetry,' where fewer electrons were emitted in the forward hemisphere compared to the backward hemisphere relative to the nuclear spins. According to parity invariance, the decay rates for electrons emitted in the forward and backward hemispheres should have been equal, as shown in Figure 15.1. However, this symmetry was violated, indicating that parity is not conserved in weak interactions.

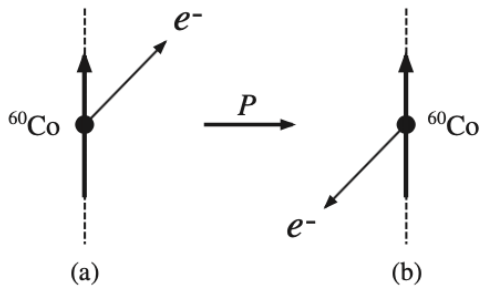

Figure 15.1: Effect of a parity transformation on ^{60}Co decay. (a) The electron is emitted in the forward direction relative to the nuclear spin. (b) Under parity transformation, the electron should have been emitted in the backward direction, but this was not observed, indicating parity violation.

15.2.2 Significance of Parity Violation

The discovery of parity violation was a watershed moment in the history of particle physics. It revealed that weak interactions are fundamentally different from strong and electromagnetic interactions, where parity is conserved. The large effect of parity violation in weak interactions is closely related to the spin structure of these interactions, which cannot be understood without considering this violation.

[1] The experiment by Wu et al. provided the first clear evidence for parity violation in weak interactions. The significance of this discovery lies in the fact that it challenged the previously held belief that parity was a universal symmetry in nature.

15.3 C-Violation in Weak Interactions

Charge conjugation (C) symmetry, which transforms particles into their corresponding antiparticles, is another fundamental symmetry in particle physics. In weak interactions, this symmetry is violated, leading to observable effects in the decay processes of particles such as muons. The close relationship between C-violation and P-violation is particularly evident in the angular distributions of decay products in these interactions.

15.3.1 Muon Decay and Charge Conjugation

In the decay of muons, specifically μ^- and μ^+ (muons and antimuons), the angular distribution of the emitted electrons (or positrons) can be described by:

$$\mu^- \to e^- + \overline{\nu}_e + \nu_\mu \tag{15.2}$$

$$\mu^+ \to e^+ + \nu_e + \overline{\nu}_\mu \tag{15.3}$$

The differential decay rate in the rest frame of the decaying particle is given by:

$$\Gamma_{\mu^\pm}(\cos\theta) = \frac{1}{2}\Gamma_\pm \left(1 - \frac{\xi_\pm}{3}\cos\theta\right) \tag{15.4}$$

where θ is the angle between the muon spin direction and the direction of the outgoing electron (or positron). The parameters $\xi_\pm$ are the asymmetry parameters, which provide a measure of C-violation. In the ideal case of C invariance, these parameters should be equal:

$$\xi_+ = \xi_- \quad \text{(C invariance)} \tag{15.5}$$

The total decay rates are related to the inverse lifetimes:

$$\tau_\pm^{-1} \equiv \int_{-1}^{+1} d\cos\theta \Gamma_{\mu^\pm}(\cos\theta) = \Gamma_\pm \tag{15.6}$$

15.3.2 Significance of Charge Conjugation Violation

The violation of charge conjugation symmetry in weak interactions is significant because it demonstrates that weak interactions do not treat particles and antiparticles symmetrically. If charge conjugation were conserved, we would expect the decay rates and angular distributions for the processes involving μ^- and μ^+ to be identical. This would imply:

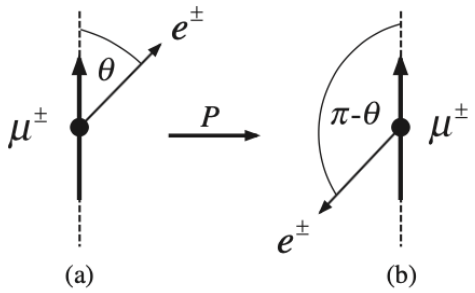

Figure 15.2: Effect of a parity transformation on the muon decays. (a) The electron is emitted in the forward direction relative to the muon spin. (b) Under parity transformation, the electron should have been emitted in the backward direction, but this is not observed, indicating parity violation.

$$\Gamma_+ = \Gamma_- \quad \text{(C invariance)} \tag{15.7}$$

and

$$\xi_+ = \xi_- \quad \text{(C invariance)} \tag{15.8}$$

Parity (P) transformation preserves the identity of particles but reverses their momenta while leaving their spins unchanged. Therefore, P invariance implies:

$$\Gamma_{\mu^\pm}(\cos\theta) = \Gamma_{\mu^\pm}(-\cos\theta) \quad \text{(P invariance)} \tag{15.9}$$

leading to:

$$\xi_\pm = 0 \quad \text{(P invariance)} \tag{15.10}$$

However, experimental results indicate that:

$$\xi_+ = -\xi_- = 1.00 \pm 0.04 \tag{15.11}$$

This measurement shows that both C invariance and P invariance are violated in muon decays, a finding that has profound implications for the understanding of weak interactions [2].

While both C and P symmetries are violated individually, their combined operation (CP) is often conserved in weak interactions, especially in leptonic decays.

[2]The observed C-violation in muon decay, alongside P-violation, underscores the unique nature of weak interactions, where these fundamental symmetries do not hold. The study of these violations provides crucial insights into the underlying principles of particle physics, particularly in the context of the Standard Model.

15.4 Principle of CP Conservation

The principle of CP conservation states that the weak interaction is invariant under the combined operation of CP, even though both C and P are separately violated. The CP operator transforms particles at rest into their corresponding antiparticles at rest. CP invariance requires that these states should have identical properties, particularly their masses.

As a direct consequence of CP invariance, certain decay processes, such as those involving muons, display identical lifetimes for particles and antiparticles. This can be expressed mathematically as:

$$\Gamma_{\mu^+}(\cos\theta) = \Gamma_{\mu^-}(-\cos\theta) \tag{15.12}$$

Thus, the total decay rates satisfy:

$$\Gamma_+ = \Gamma_- \quad \text{(CP invariance)} \tag{15.13}$$

and the asymmetry parameters are related as:

$$\xi_+ = -\xi_- \quad \text{(CP invariance)} \tag{15.14}$$

15.4.1 Implications for CP Invariance

The mathematical expressions derived from the principle of CP conservation are crucial in explaining the behavior of particles in weak interactions. For example, in muon decays, the observed decay rates and angular distributions are consistent with CP invariance, which retains the symmetry between particles and antiparticles.

While the equations:

$$\Gamma_{\mu^+}(\cos\theta) = \Gamma_{\mu^-}(-\cos\theta) \tag{15.15}$$

$$\Gamma_+ = \Gamma_- \tag{15.16}$$

$$\xi_+ = -\xi_- \tag{15.17}$$

confirm CP invariance in leptonic decays, it is important to note that CP invariance is not always preserved in weak interactions involving quarks. The weak interactions of quarks, particularly in processes involving neutral kaons and B mesons, show observed CP violations. These violations, though confined to specific decays, provide crucial insights into the underlying principles of weak interactions.

15.5 CP Violation in Weak Interactions

CP violation refers to the violation of the combined symmetry of charge conjugation (C) and parity (P) in certain weak interactions. One of the most studied cases of CP violation occurs in the neutral kaon system, which provides significant insights into the behavior of weak interactions.

15.5.1 Neutral Kaon Mixing and CP Violation

The two neutral kaon states, $K^0(498) = d\bar{s}$ and $\overline{K}^0(498) = s\bar{d}$, have strangeness $S = +1$ and $S = -1$, respectively. Since strangeness is not conserved in weak interactions, these states can be converted into each other by higher-order weak processes, a phenomenon known as $K^0 - \overline{K}^0$ mixing.

$$K^0 \leftrightarrow \overline{K}^0 \tag{15.18}$$

This mixing is in contrast with most other particle-antiparticle systems, for which such transitions are forbidden because the particle and its antiparticle differ by quantum numbers that are conserved in all known interactions. However, for neutral kaons, there is no conserved quantum number to distinguish the two states when weak interactions are taken into account, and the observed physical states correspond to linear combinations of them:

$$|K_1\rangle = \frac{1}{\sqrt{2}}(|K^0\rangle + |\overline{K}^0\rangle) \tag{15.19}$$

$$|K_2\rangle = \frac{1}{\sqrt{2}}(|K^0\rangle - |\overline{K}^0\rangle) \tag{15.20}$$

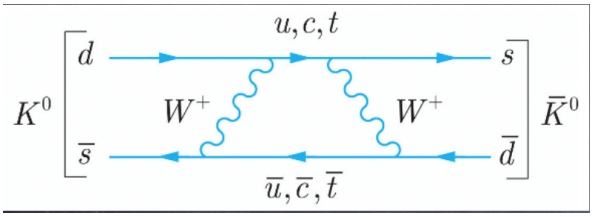

Figure 15.3: Neutral kaon mixing through higher-order weak processes. The diagram illustrates the transition between K^0 and $\overline{K}^0$ states, a process that leads to CP violation in the kaon system.

15.5.2 The CKM Matrix and CP Violation

In 1973, Kobayashi and Maskawa extended the understanding of CP violation by introducing the Cabibbo-Kobayashi-Maskawa (CKM) matrix, which tracks the weak decays of three generations of quarks. The CKM matrix provides a mechanism for CP violation in the Standard Model and is essential in explaining the observed phenomena in quark decays.

$$\begin{bmatrix} d' \\ s' \\ b' \end{bmatrix} = \begin{bmatrix} V_{ud} & V_{us} & V_{ub} \\ V_{cd} & V_{cs} & V_{cb} \\ V_{td} & V_{ts} & V_{tb} \end{bmatrix} \begin{bmatrix} d \\ s \\ b \end{bmatrix} \tag{15.21}$$

The CKM matrix describes the probability of transition from one quark flavor to another and is central to the study of CP violation in the quark sector.

CKM matrix

In 1973, observing that CP-violation could not be explained in a four-quark model, Kobayashi and Maskawa generalized the Cabibbo matrix into the Cabibbo–Kobayashi–Maskawa matrix (or CKM matrix) to keep track of the weak decays of three generations of quarks:[5]

$$\begin{bmatrix} d' \\ s' \\ b' \end{bmatrix} = \begin{bmatrix} V_{\mathrm{ud}} & V_{\mathrm{us}} & V_{\mathrm{ub}} \\ V_{\mathrm{cd}} & V_{\mathrm{cs}} & V_{\mathrm{cb}} \\ V_{\mathrm{td}} & V_{\mathrm{ts}} & V_{\mathrm{tb}} \end{bmatrix} \begin{bmatrix} d \\ s \\ b \end{bmatrix}.$$

On the left are the weak interaction doublet partners of down-type quarks, and on the right is the CKM matrix, along with a vector of mass eigenstates of down-type quarks. The CKM matrix describes the probability of a transition from one flavour j quark to another flavour i quark. These transitions are proportional to $|V_{ij}|^2$.

As of 2023, the best determination of the individual magnitudes of the CKM matrix elements was:[6]

$$\begin{bmatrix} |V_{ud}| & |V_{us}| & |V_{ub}| \\ |V_{cd}| & |V_{cs}| & |V_{cb}| \\ |V_{td}| & |V_{ts}| & |V_{tb}| \end{bmatrix} = \begin{bmatrix} 0.97373 \pm 0.00031 & 0.2243 \pm 0.0008 & 0.00382 \pm 0.00020 \\ 0.221 \pm 0.004 & 0.975 \pm 0.006 & 0.0408 \pm 0.0014 \\ 0.0086 \pm 0.0002 & 0.0415 \pm 0.0009 & 1.014 \pm 0.029 \end{bmatrix}.$$

Using those values, one can check the unitarity of the CKM matrix. In particular, we find that the first-row matrix elements give: $|V_{\mathrm{ud}}|^2 + |V_{\mathrm{us}}|^2 + |V_{\mathrm{ub}}|^2 = 0.9985 \pm 0.0007$;

The difference from the theoretical value of 1 poses a tension of 2.2 standard deviations. Non-unitarity would be an indication of physics beyond the Standard Model.

The choice of usage of down-type quarks in the definition is a convention, and does not represent a physically preferred asymmetry between up-type and down-type quarks. Other conventions are equally valid: The mass eigenstates u, c, and t of the up-type quarks can equivalently define the matrix in terms of *their* weak interaction partners u′, c′, and t′. Since the CKM matrix is unitary, its inverse is the same as its conjugate transpose, which the alternate choices use; it appears as the same matrix, in a slightly altered form.

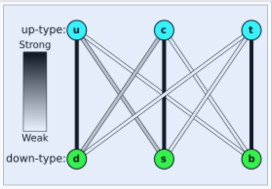

A pictorial representation of the six quarks' decay modes, with mass increasing from left to right.

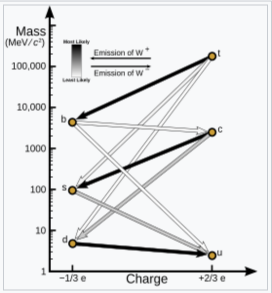

A diagram depicting the decay routes due to the charged weak interaction and some indication of their likelihood. The intensity of the lines is given by the CKM parameters

Figure 15.4: Pictorial representation of the CKM matrix and its role in quark decays. The matrix elements dictate the mixing between different quark generations, leading to CP violation.

The precise measurements of the CKM matrix elements have provided insights into the degree of CP violation in the Standard Model. Understanding the CKM matrix and its implications is crucial for explaining the matter-antimatter asymmetry observed in the universe.

Example: Determination of $|V_{cb}|$ from Semileptonic Decays

Consider the determination of the CKM matrix element $|V_{cb}|$ using the inclusive semileptonic decays of B mesons to charm. The inclusive determinations use the semileptonic decay rate measurement, together with moments of the lepton energy and the hadronic invariant mass spectra.

The value of $|V_{cb}|$ is determined as follows:

$$|V_{cb}| = (42.2 \pm 0.8) \times 10^{-3}. \tag{15.22}$$

This value is obtained from an average of measurements involving B mesons produced from Z^0 decays at

LEP and from e^+e^- colliders operated at the $\Upsilon(4S)$ resonance. The measurements from LEP benefit from the large boost of B mesons, allowing the determination of moments across the entire phase space, while the high statistics at B factories provide more precise determinations.